Microarray analysis of bone marrow lesions in osteoarthritis demonstrates upregulation of genes implicated in osteochondral turnover, neurogenesis and inflammation

Anasuya Kuttapitiya[1], Lena Assi[1], Ken Laing[1], Caroline B Hing[3], Philip Mitchell[3], Guy Whitley[2], Abiola Harrison[1], Franklyn Howe[2], Vivian Ejindu[3], Christine Heron[3], Nidhi Sofat[1]

1. Institute for Infection and Immunity, St George's, University of London, Cranmer Terrace, London, SW17 ORE
2. Molecular and Clinical Sciences Research institute, St George's, University of London, Cranmer Terrace, London, SW17 ORE
3. St George's University Hospitals NHS Foundation Trust, Blackshaw Road, London, SW17 OPQ

Address for Correspondence: Dr Nidhi Sofat, Mail point J1A, St George's, University of London, Cranmer Terrace, London SW17 ORE. Email: nsofat@sgul.ac.uk

Abstract

***Objective*:** Bone marrow lesions (BML) are well described in osteoarthritis (OA) using magnetic resonance imaging (MRI) and are associated with pain but little is known about their pathological characteristics and gene expression. We evaluated BMLs using novel tissue analysis tools to gain a deeper understanding of their cellular and molecular expression.

***Methods*:** We recruited 98 participants, 72 with advanced OA requiring total knee replacement (TKR), 12 with mild OA and 14 non-OA controls. Participants were assessed for pain (using WOMAC) and with a knee MRI (using MOAKS). Tissue was then harvested at TKR for BML analysis using histology and tissue microarray.

***Results*:** The mean (SD) WOMAC pain scores were significantly increased in advanced OA 59.4 (21.3) and mild OA 30.9 (20.3) compared to controls 0.5 (1.28) ($p<0.0001$). MOAKS showed all TKR tissue analysed had BMLs, and within these lesions, bone marrow volume was starkly reduced being replaced by dense fibrous connective tissue, new blood vessels, hyaline cartilage and fibrocartilage. Microarray comparing OA BML and normal bone found a significant difference in expression of 218 genes ($p<0.05$). The most upregulated genes included stathmin 2, thrombospondin 4, matrix metalloproteinase 13 and Wnt/Notch/catenin/chemokine signalling molecules that are known to constitute neuronal, osteogenic and chondrogenic pathways.

***Conclusion*:** Our study is the first to employ detailed histological analysis and microarray techniques to investigate knee OA BMLs. BMLs demonstrated areas of high metabolic activity expressing pain sensitisation, neuronal, extracellular matrix and pro-inflammatory signalling genes which may explain their strong association with pain.

Introduction

Osteoarthritis (OA) is the most common form of arthritis worldwide affecting more than 27 million adults in the USA alone (1) and is a major cause of pain and functional disability. OA prevalence is set to rise globally with aging populations accompanied by the rising epidemic of obesity (2). OA most commonly affects large weight-bearing joints, affecting the knees in up to 37% of adults over 60 (1). Pain is a major symptom for people with OA, with 16.7% of US adults aged 45 and above reporting pain as a predominant problem (1).

Pain in OA is thought to arise from several structures within the arthritic joint, including the synovium (from which prostaglandins, leukotrienes and inflammatory mediators are released), joint effusions, joint capsule involvement, tendon and muscle weakness which all contribute to pain and reduced function (3). Synovitis is often observed by magnetic resonance imaging (MRI) in OA and strongly correlates with pain (4). Cartilage degradation is one of the hallmarks of OA disease (5) and exposes the structures from which pain is most likely arising as cartilage is an avascular, aneural structure composed largely of extracellular matrix (ECM) embedded sparsely with chondrocytes. Recent interest has grown in the importance of bone marrow lesions (BMLs) in relation to pain in OA. Epidemiological studies have shown a strong correlation between BMLs observed by MRI and OA-related knee pain in several large cohorts (6, 7), with an odds ratio of 3.2 for the association of BMLs with pain. The data outlined above demonstrate the multifactorial nature of OA and how pain mechanisms are supported by the biopsychosocial model of pain.

Recently, BMLs have been shown to be a very early biomarker of joint damage in OA (6, 7) with descriptions of their histology and histomorphometry. However, no previous

transcriptomic studies of BMLs in OA are described. In the current study we describe novel findings demonstrating BMLs have features of angiogenesis, fibrosis, new cartilage formation and increased bone turnover with disruption of the physiological osteochondral interface. Whole transcriptomic analysis of BML regions found upregulated expression of genes involved in neurogenesis, pain sensitisation, chemokine and cytokine signalling as well as cartilage remodelling pathways.

Materials and Methods

All study procedures were carried out after ethical approval was granted (Health Research Authority approval number 12/LO/1970 and clinical trials.gov identifier NCT02603939). Participants attending the South London Elective Orthopaedic Centre were recruited at assessment for TKR, comprising the “advanced OA group”. For the “mild OA” group, participants were recruited from rheumatology clinics at St George’s University Hospitals NHS Foundation Trust. For bone tissue controls, participants undergoing surgery following trauma, amputation or trochleoplasty were recruited (approval number 09/H0806/45) with no clinical or radiographic arthritis. Blood and urine samples were also obtained with full consent for biomarker studies.

Study criteria. Eligibility for participation included age of 35-90 years, presenting with pain and fulfilling ACR criteria for the diagnosis of knee OA (8). Participants continued to experience pain despite treatment for OA (9). All participants underwent baseline knee radiography to confirm knee OA with a Kellgren-Lawrence grade of greater than 2 in the affected tibio-femoral knee joint (10).

***Clinical data collection*.** All scores were collected for participants with advanced OA and mild OA. For controls WOMAC was not collected as participants underwent

different surgeries. The primary pain score was the Western Ontario and McMaster Universities Osteoarthritis Index (WOMAC) with sub-scales for pain, stiffness and function (11). Participants were asked to score based on symptoms in the last 48 hours. Data were also collected for body mass index (BMI), Visual Analogue Scale (VAS) pain rating 0 - 10 (12) and the Hospital Anxiety and Depression Scale (HADS) (13).

Molecular methods. Total RNA was isolated from approximately 200mg of bone tissue. Amplified labelled cRNA samples (600ng) were hybridized to Agilent whole human genome 60k microarray chips. Array signal intensities were analysed by the Agilent Gene-Spring GX software. Significant differentially expressed entities between bone samples from healthy controls and OA participants were selected using a union of a student's/moderated t-test corrected for multiple comparisons with the Bonferroni correction ($P < 0.05$). Further methodical details are provided in the supplementary methods.

Statistical Analysis

Data was anonymised for all analyses independently by the research team who were not involved in diagnosing or treating the study participants. To detect significant differences between groups at $p < 0.05$, recruitment of at least 80 subjects was required and we achieved n=98 participants. Graphpad Prism version 7 was used for all analyses and significance set at $p < 0.05$ for all analyses. For microarray statistical analysis refer to supplementary methods.

Results

Demographic data showed that our participants were representative of a knee OA population. Knee OA participants who underwent TKR had a high BMI and high pain scores measured by WOMAC (Table 1). The mean (SD) WOMAC pain scores were significantly increased in advanced OA 59.4 (21.3) and mild OA 30.9 (20.3) compared to controls 0.5 (1.28) ($p<0.0001$), showing the advanced OA group had significantly more severe pain and functional impairment.

A mixture of OA participants was identified and they were classified as severe or mild based on MRI. In the advanced OA group, 81.3% of participants had up to 33% of the bone volume (MOAKS score 1) forming a BML in at least one of the 21 measured regions, in addition to significant levels of synovitis and cartilage damage (Table 1). MRI scans found BML areas to be invariably associated with regions of established cartilage damage, particularly in medial tibial regions, which were the focus of our tissue and microarray to maintain consistency of anatomical tissue lesions analysed. We found that 37.5% of grade 1 and 2 BML were in the medial tibial compartment, with 12.5% in the lateral tibial compartment. The remainder were distributed in the femur, trochlea and patella. For microarray, 50% samples were localised in the medial tibial compartment, 35.7% were found in the lateral tibial compartment and 14.2% crossed both tibial compartments.

Trends for WOMAC pain with individual MOAKS modalities showed higher WOMAC pain scores were associated with significantly greater cartilage damage in advanced and mild OA (Supplementary Figure 1). There was also a trend of increasing WOMAC pain with worsening MOAKS-scored synovitis, although these correlations did not reach statistical significance.

Histological analysis showed most normal bone marrow was adipocytic with adipocytes being the primary bone lining cells (Figure 1). The bone volume fraction was starkly reduced in BML areas, with marrow replaced by new blood vessels, dense fibrous connective tissue, hyaline cartilage and fibrocartilage. Areas of aggressive resorption were found at the periphery of BML zones alongside regions of cartilaginous aggregates found at least 2 mm deep to the articular surface embedded within the bone compartment. Regions of vascular proliferation with fibrocartilage were interspersed with areas of *de novo* cartilage formation. Other BML regions exhibited a cellular infiltrate working through the osteoid network. Histological quantification found the BML group had increased vascular proliferation, cellular infiltration and trabecular thickening when compared to the NBML group ($p<0.05$).

Whole transcriptomic analysis identified 218 entities to be significantly differentially expressed between the OA BML and control bone samples ($p<0.05$) (Figure 2, 3). The most highly upregulated genes were stathmin 2 (*STMN2*), ATP-binding cassette protein (*ABCB5*), thrombospondin 4 (*THBS4*), matrix metalloproteinase 13 (*MMP13*) and chromosome 21 open reading frame (*C21orf37*), which are genes involved in diverse functions including bone remodelling, pain sensitisation and matrix turnover (see discussion). The most down regulated genes included haemoglobin (*HBG1*), S100 calcium binding protein A12 (*S100A12*), hemogen (*HEMGN*), pro-platelet basic protein [(chemokine C-X-C) motif ligand 7] (*PPBP*) and delta amino levulinate synthase 2 (*ALAS2*) (Table 2, supplementary data Table 1 for full list).

Among other significantly upregulated genes were the EGF-like domain (*EGFL6*) which is involved in cell adhesion, apoptosis and calcium binding, collagen type XVI (*COL16A1*) with functions in ECM organisation, cell adhesion and integrin mediated

signalling, G protein coupled receptor (*GPR158*) which facilitates signal transduction and binds hormones/neurotransmitters and ATPase H+ transporting lysosomal (*ATP6V0D2*) gene expressed at axon termini and synaptic vesicles that is implicated in neuron projection. We also found upregulation of the DIRAS family, GTP-binding RAS-like 2 (*DIRAS2*) which is a Ras GTPase implicated in neurodegeneration. PC4 and SFRS1 interacting protein 1 (*PSIP1*) were also identified and are molecules involved in neuro-epithelial stem cell differentiation, neurogenesis and apoptosis. Neuronal tyrosine phosphorylated phosphoinositide-3-kinase adaptor 2 (*NYAP2*) was also detected, which is a gene involved in neuronal development, interacting with WAVE1 proteins and is implicated in cytoskeletal modelling. We also found catenin (cadherin-associated protein) (*CTNND2*) upregulation, an adhesive junction associated protein implicated in bone, pain sensitisation, brain development and cancer formation.

Gene ontology analysis identified 166 of the 218 significantly differentially regulated entities to be associated with 59 canonical pathways. The angiogenic, Alzheimer disease-presenilin pathway, EGF/FGF/gonadotrophin signalling, inflammation mediated by chemokine and cytokine signalling with PDGF/Notch/VEGF and Wnt signalling pathways were a few of which had the greatest number of entities related.

Quantitative polymerase chain reaction (qPCR) analysis confirmed *STMN2*, *MMP13* and *THBS4* were significantly upregulated in BML regions compared to the control comparator group. *THBS4* and *STMN2* were the most highly upregulated genes between the BML and control bone groups ($p<0.0001$), reflecting comparable results to the microarray (Figure 4). *MMP13* and *STMN2* were upregulated within BML regions compared to NBML matched regions ($p<0.0001$). However *THBS4* was found

to be most upregulated in the NBML compared to both BML and control groups. Serum STMN2 levels were not significantly increased in mild/ advanced OA groups compared to controls. Protein quantification of STMN2 in BML tissue found control bone to have higher presence of STMN2 compared to BML bone ($p<0.0001$). Functional significance of *MMP13* protein activity, one of the highest array-expressed genes, found a significant increase in urine CTX-II levels i.e. cleavage products of type II collagen, in the advanced OA group compared with mild OA and control groups ($p<0.001$) (Supplementary Figure 2).

Discussion

BMLs have been well described by MRI in knee OA (6, 7, 14), but very little is known about their transcriptomic expression. To our knowledge, our study is the first to use a multimodal approach with MRI to locate knee OA BMLs, followed by detailed histological analysis and whole transcriptomic techniques for a multivariate interrogation of the changes seen within BMLs.

Bone marrow signal changes were first described on MRI by Wilson *et al.* who used the term 'bone marrow edema' (BME) to describe MRI findings in painful joints (19). Studies so far have focused on acquiring data from patients undergoing joint surgery of the knee and hip. Zanetti *et al.* determined histologically that BMLs contained normal fatty marrow with marrow necrosis, necrotic or remodelled trabeculae, oedema and bone marrow bleeding (20). The same group matched MRI changes to BML abnormalities in participants undergoing TKR and found regions of normal tissue alongside bone marrow fibrosis, oedema and bleeding. In a hip and knee OA study, Hunter *et al.* reported increased bone volume fraction but decreased tissue mineral density within BML using light microscopy (21). Samples from the lesion area showed increased trabecular thickness, with granulation, oedema, necrosis, fibrinoid deposition and hyperplasia of blood vessels. Taljanovic reported one of the largest histological studies of hip OA BML, where regions of fibrosis and microfracture formation at different stages of healing were observed (22). Leydet-Quilici *et al*. also described oedema, necrosis and fibrosis within BML biopsies (23). Using MRI, Roemer *et al.* previously demonstrated that progression of disease and the development of BMLs correlated with an increased risk of cartilage loss within the same subregion and that regions without BMLs are associated with decreased risk of cartilage loss (24), changes which our work supported. Carrino *et al*. (25) reported

87% of subchondral cysts were associated with BML abnormalities which our analysis confirmed on MRI and by histology. In comparison to other studies, our detailed MRI matching with histological techniques allowed improved visualisation of BMLs, with direct observation of areas appearing as BML-associated cystic structures on MRI and transcriptomic expression. We found higher WOMAC pain scores with greater MOAKS-measured cartilage damage, as suggested by previous studies (7).

In our study, cystic BML areas were surrounded by regions of fibrosis, infiltration by inflammatory cells and vascular proliferation. Previous hypotheses that BMLs could be precystic, but that not all BMLs become cystic is also supported by our histological findings, where we observed cystic structures within the areas defined as cysts using MRI, but also adjacent to areas of fibrocartilage, vascular proliferation, chondrogenesis and amorphous tissue deposition. We observed new cartilage forming deep within the subchondral bone compartment. The new cartilage tissue within the BML could be arising from mesenchymal stem cells (MSCs) in the marrow, which is seen by other groups (26). Campbell *et al.* reported an altered phenotype of MSCs in hip OA BMLs, showing BML-derived MSCs undergo osteochondral angiogenesis and have lower proliferation and mineralisation capacities (27).

From our microarray, the highest upregulated gene was *STMN2*, a phosphoprotein involved in regulating microtubule function, responsiveness to nerve growth factor (NGF), neuronal growth and osteogenesis (28). Upregulation of *STMN2* within BML could lead to new neuronal structures and expansion of the BML in OA, thereby causing pain (29). Stathmin 2 protein expression was higher in normal than BML bone, which could reflect increased stathmin 2 turnover in OA BMLs

We also identified neuronal markers including thrombospondin 4 (*THBS4)*, implicated in the inflammatory response to CNS injury, presynaptic hypersensitivity and neuropathic pain states (30). In animal models of pain sensitisation, *THBS4* levels are increased locally in dorsal root ganglion neurons and contribute to pain behaviour, which can be inhibited by the calcium channel modulator gabapentin (31).

Other upregulated genes involved in neuronal morphogenesis included *ATP6V0D2*, *PSIP1*, *NYAP2*, FERM and PDZ containing 4 (*FRMPD4*), implicated in CNS development and pain states (32, 33). Extracellular matrix genes were also represented in the array, including *MMP13* and collagens, *COL16A1*, fibronectins and growth factors which are known to be bound within the ECM (34).

Our data demonstrate that BMLs are regions of high metabolic activity with increased cell turnover, bone remodelling, neuronal and inflammatory gene signatures. Gene ontological analysis revealed canonical pathways involved in chemokine, integrin and cytokine signalling. We found neuro-development and pain pathway signalling represented by the Alzheimer's, Notch, catenin, Wnt pathways alongside VEGF and angiogenic pathway expression. Work by Hopwood *et al.* (35) and Chou *et al.* (36) analysing the gene expression profile of OA bone also found expression of bone remodelling signalling pathways including Wnt, transforming growth factor (*TGF-β*) and bone morphogenic protein (*BMP*) and bone remodelling molecules such as periostin (*POSTN*) and leptin (*LEP*). Kusumbe *et al.* described how growth of blood vessels in bone and osteogenesis are coupled, proposing that type H endothelial cells mediate local growth of the vasculature and provide specific signals for perivascular osteoprogenitors (37). The same group reported that endothelial Notch activity promotes angiogenesis and osteogenesis in bone (38). We also demonstrated *OMD*

in our BML tissue: Ninomiya *et al.* showed that osteoclast activity induces *OMD* expression in bone, suggesting BMLs represent areas of active bone remodelling (39).

The expression of both osteogenic and angiogenic genes along with the tissue changes we identified may suggest that vascular proliferation and bone formation are likely to be coupled in BML formation. Since blood vessels are formed within neurovascular bundles, it is likely that increased neuronal pathway gene expression including *STMN2*, *THBS4*, *PSIP1*, *NYAP2* and catenin, which were among some of the most highly expressed genes from our BML analysis, are implicated in neural pathway development, new nerve formation and pain mediation in BML tissue.

Our array also identified molecules within the Wnt signalling pathway, including catenin. Other studies have demonstrated a critical role for Wnt signalling in the production and persistence of neuropathic pain after nerve injury and bone cancer (40). Rodent models show that in nerve injury and bone cancer pain models, respectively, Wnt signalling is activated, which may contribute to pain by regulating pro-inflammatory cytokines IL-18 and TNF-α, as well as NR2B and subsequent Ca2+-dependent signals in the dorsal horn. We found a high representation of the inflammatory chemokines and cytokine signalling; other groups have also identified chemokines in OA pain e.g. *CCR2* was recently reported to mediate pain in a murine model of OA (41). Our data suggest that chemokine pathway molecules could be pain sensitisers in BMLs. Walsh *et al.* showed that OA neurovascular changes at the osteochondral junction, including vessels and both sensory and sympathetic nerves breaching the tidemark, could possibly be a source of joint pain (42). The genes we have identified in our BML transcriptome support the hypothesis of neurovascular gene upregulation in BML tissue.

One of our most highly expressed genes was *MMP13*, an enzyme expressed in cartilage, involved in regulating ECM turnover and cartilage destruction in OA (43). Our data showed that type II collagen degradation products were increased in urine from our advanced OA population. The *de novo* cartilage formation observed within BMLs, coupled with the increased transcriptomic expression of *MMP13* observed using microarray and the detection of MMP13 cleavage products, could suggest recapitulation of the embryonic bone development phenotype within OA BML regions. Limitations of our study included the sample size for microarray, which although on a standard format of 24 samples, will benefit from larger studies. Future work for protein evaluation of the genes identified is needed, investigating which cells within BMLs are responsible for producing the genes identified and how BMLs develop with respect to the pathological changes identified in OA over time. Although we did not identify NGF, we found genes in neurotrophin pathways, including stathmin 2, which increases responsiveness to NGF (28), syntaxin, which regulates brain-derived neurotrophic factor (BDNF) (44) and pituitary adenylate cyclase-activation polypeptide (PACAP), implicated in neuronal development (45).

In conclusion, our work demonstrates that BMLs are regions of high metabolic activity, with expression of genes involved in neuronal development, pain, extracellular matrix turnover, cartilage/bone formation and angiogenesis. Our findings contribute to understanding of OA pathogenesis and could help lead to the development of new diagnostic tools and future therapies for this most common arthritic disease.

3000 words

Competing interest: None declared

Acknowledgements

We express our sincere gratitude to all patients who participated in this study.

Collaborators on study team: St George's University Hospitals NHS Foundation Trust - Dr Virinderjit Sandhu, Dr Katie Moss, Dr Arvind Kaul, Dr Patrick Kiely (Co-Investigators); St George's, University of London: Ms Debbie Rolfe (Regulatory Manager), Dr Irina Chis Ster (Statistician) and Professor Mary Sheppard (Consultant Pathologist).

Contributors: NS wrote the study protocol and associated documents, coordinated the implementation of the study, collated and managed the study data, conducted data analysis and drafted the manuscript. LA, KL, GW, CH, PM, SB supported AK and NS in the study design, data collection study implementation and analysis. VE and CH interpreted the MRI knee scores for data analysis

All authors contributed to the interpretation of study findings, serial revisions of the manuscript and final approval of the submitted version.

Ethics approval - This study was approved and implemented in accordance with Good Clinical Practice guidelines. All participants gave written informed consent.

Funding

Supported by the Rosetrees' Trust (Grant number M11-F2) and by the UK National Institute for Health Research (NIHR) Clinical Research Network. A Kuttapitiya's work was also supported by St George's, University of London and Neusentis through a PhD studentship award. The views expressed are those of the author(s) and not necessarily those of the NHS, the NIHR or the Department of Health.

Figures and Tables

Figure 1. **(A)** Coronal plane of MRI scan visualising BML and associated cyst. **(B)** Axial plane of MRI scan presenting BML and associated cyst. **(C)** Macroscopic view of tibial BML and cystic area. **(D)** Image of cross section cut through BML and cyst localised by MRI revealing a gelatinous aggregate. **(E)** H&E staining of cystic region presenting cellular infiltrate in marrow spaces. **(F)** H&E staining of subchondral cyst forming. **(G)** H&E staining of BML region with vascular proliferation and cellular infiltration. **(H)** H&E staining of BML visualising a chondrification centre near the tidemark. **(I)** H&E staining of adipocyte in bone compartment with a soft tissue infiltrate working through osteoid network. **(J)** H&E staining of BML showing areas of thickened trabecular adjacent to thinning trabeculae. **(K)** H&E staining of BML demonstrating areas of fibrotic cartilage formation within the subchondral bone compartment. **(L)** Quantification of histology analysing 50 BML fields of view (FOV) and 40 non-BML (NBML) FOV for blood vessels (BV), cartilage within bone compartment (Cart), cysts (Cys), myxoid/fibrous tissue (M/F), cellular infiltrate (Inf) and trabecular thickening (TT) (n = 4). A percentage for the presence of each histological feature was determined for each group. Significance was tested between the groups using Friedman test (*$p<0.05$). **(M)** Magnification of each histological change within the bone compartment: BV within subchondral bone, Cart within bone compartment with a chondrification

centre, Cys within subchondral bone, M/F adjacent to subchondral bone, Inf within the osteoid network and TT.

Figure 2. (A) Bar chart presenting the most significantly upregulated and downregulated entities by fold change (FC). 128 entities were found to be upregulated and 90 were downregulated. The mean WOMAC pain score in the OA microarray group was 61.4 and all subjects in the OA array group had a MOAKS BML score of at least 1, with cartilage and synovitis scores of at least 2 (B) Pearson's correlation hierarchical clustering of 218 genes clearly segregating the OA BML group from the control group.

Figure 3. (A) Gene ontology analysis of 218 differentially expressed entities found 166 genes associated with 59 canonical pathways. Pie chart of the 24 predominant pathways identified. The main significant correlation for WOMAC pain with gene correlation was for MMP-13 ($p<0.05$). (B) Network analysis was performed on the differentially expressed genes by ingenuity pathway analysis (IPA).

Figure 4. qPCR validation for Stathmin 2 (*STMN2*), Thrombospondin 4 (*THBS4*), Matrix Metalloproteinase 13 (*MMP13*) and Osteomodulin (*OMD*) of OA BML compared non-BML tissue and control bone. *STMN2*, *THBS4* and *MMP13* were selected as they were among the most upregulated genes from the microarray. Osteomodulin was selected as a bone-specific marker as it is involved in bone homeostasis (**$p<0.005$, ***$p<0.0005$).

Tables

Table 1: Demographics showing characteristics of study population
Key. Data presented as means and standard deviations. MOAKS: MRI Knee Osteoarthritis Score. WOMAC: Western Ontario and McMaster Universities Osteoarthritis Index. HADS: Hospital Anxiety and Depression Scale

Table 2. Summary of the top differentially expressed entities between the OA BML and non-OA control groups using whole transcriptomic analysis.

Supplementary Section

Supplementary Methods. Methods for MRI, histology, microarray, qPCR, Western blot and ELISA.

Supplementary Figure 1. (A) Correlation of WOMAC pain with MOAKS BML size, cartilage damage (CD) and synovitis (Syn) grade 1 between advanced OA and mild OA groups. Grade 1 severity was selected for each MOAKS modality for comparison between groups. Mann Whitney U was used to compare significance between advanced and mild OA groups B. Table summarising bivariate correlation analysis between MOAKS parameters and WOMAC pain using Spearman's rank correlation coefficient statistical testing. C. Time course of WOMAC pain with MOAKS BML size, cartilage damage (CD) and synovitis (Syn) score over 12 months' study period (n=62).

Supplementary Figure 2. A. Measurement of Stathmin 2 expression by serum ELISA in control, mild OA and advanced OA samples; B. Protein expression of stathmin 2 measured by Western blotting in BML tissue extracts and control non-OA extracts (p***<0.0005); C. Measurement of urinary CTX-II C-telopeptides by ELISA in advanced OA, mild OA, and healthy control subjects (p***<0.0005).

Supplementary Data Table 1. Full list of differentially expressed entities between OA BML and non-OA control group. Legend: Accession #: Accession Number. Symbol: Entity Symbol. ↑↓: Regulation. Abs FC: Absolute Fold Change. Log FC: Log transformed Fold Change. P Value[a]: Adjusted Student T-test P value for microarray corrected for multiple testing by the Bonferroni FWER method. P Value[b]: Adjusted Moderated T-test P value for microarray corrected for multiple testing by the Bonferroni FWER method.

References

1. Lawrence RC, Felson DT, Helmick CG et al. Estimates of the prevalence of arthritis and other rheumatic conditions in the United States. Part II. Arthritis Rheum. 2008; 58(1): 26-35

2. Nicholls E, Thomas E, van der Windt DA, Croft PR, Peat G. Pain trajectory groups in persons with, or at high risk of, knee osteoarthritis: findings from the Knee Clinical Assessment Study and the Osteoarthritis Initiative. Osteoarthritis Cartilage. 2014 22(12): 2041-50.

3. Sofat N, Ejindu V, Kiely P. What makes OA painful? The evidence for peripheral and central pain processing Rheumatology, 2011, 50(12):2157-65

4. Roemer FW, Kassim Javaid M, Guermazi A, et al. Anatomical distribution of synovitis in knee osteoarthritis and its association with joint effusion assessed on non-enhanced and contrast-enhanced MRI. Osteoarthritis Cartilage 2010; 18: 1269-74

5. Roy S, Meachim G. Chondrocyte ultrastructure in adult human articular cartilage. Ann Rheum Dis. 1968; 27: 544-58

6. Felson DT, Chaisson CE, Hill CL, Totterman SM, Gale ME, Skinner KM, Kazis L, Gale DR. The association of bone marrow lesions with pain in knee osteoarthritis. Ann. Internal Med.2001; 134: 541-549

7. Sowers MF, Hayes C, Jamadar D et al. Magnetic resonance-detected subchondral bone marrow and cartilage defect characteristics associated with pain and X-ray defined knee osteoarthritis. Osteoarthritis Cartilage, 2003; 11: 387-93

8. Altman R, Asch E, Bloch D, Bole G, Borenstein D, Brandt K, et al. The American College of Rheumatology criteria for the classification and reporting of osteoarthritis of the knee. Arthritis Rheum 1986; 29: 1039-1049

9. NICE guidelines 'Osteoarthritis: Care and Management', https://www.nice.org.uk/guidance/cg177

10. Kellgren JH, Lawrence JS. Radiological assessment of osteo-arthrosis. Ann Rheum Dis 1957; 16(4): 494-502

11. Bellamy N, Hochberg M, Tubach F, Martin-Mola E, Awada H, Bombardier C, Hajjaj-Hassouni N, Logeart I, Matucci-Cerinic M, van de Laar M, van der Heijde D, Dougados M. Development of multinational definitions of minimal clinically important improvement and patient acceptable symptomatic state in osteoarthritis. Arthritis Care Res (Hoboken) 2015; 67(7): 972-80

12. Dworkin RH, Turk DC, Farrar JT, Haythornthwaite JA, Jensen MP, Katz NP. Core outcome measures for chronic pain clinical trials: IMMPACT recommendations. Pain 2005; 113: 9-19

13. Bjelland I, Dahl AA, Haug TT, Neckelmann D. The validity of the Hospital Anxiety and Depression Scale: an updated literature review. Journal of Psychosomatic Research. 2002; 52(2): 69-77

14. Hunter DJ, Guermazi A, Lo GH, Grainger AJ, Conaghan PG, Boudreau RM, Roemer FW. Evolution of semi-quantitative whole joint assessments of knee OA: MOAKS (MRI Osteoarthritis Knee Score). Osteoarthritis Cartilage 2011; 19(8): 990-1002

15. RNeasy mini Hand book isolation kit. Qiagen. Fourth Edition, June 2012. https://www.qiagen.com/es/resources/resourcedetail?id=14e7cf6e-521a-4cf7-8cbc-bf9f6fa33e24&lang=en

16. Microarray-Based Gene Expression Analysis. Version 6.9.1. December 2015. https://www.agilent.com/cs/library/usermanuals/Public/G2505-90019_ScannerC_User.pdf

17. Mi H, Poudel S, Muruganujan A, Casagrande JT, Thomas PD. PANTHER version 10: expanded protein families and functions and analysis tools. Nucleic Acids Res 2016; 44(D1): D336-42

18. Garnero P, Piperno M, Gineyts E, Christgau S, Delmas PD, Vignon E. Cross sectional evaluation of biochemical markers of bone, cartilage and synovial tissue metabolism in patients with knee osteoarthritis: relations with disease activity and joint damage. Ann Rheum Dis. (2001); 60: 619-26

19. Wilson AJ, Murphy WA, Hardy DC, Totty WG. Transient osteoporosis: transient bone marrow edema? Radiology 1988; 167(3): 757-60

20. Zanetti M, Bruder E, Romero J, Hodler J. Bone marrow edema pattern in osteoarthritic knees: correlation between MR imaging and histologic findings. Radiology. 2000;215:835–840.

21. Hunter DJ, Gerstenfeld L, Bishop G, Davis AD, Mason ZD, Einhorn TA, Maciewicz RA, Newham P, Foster M, Jackson S, Morgan EF. Bone marrow lesions from osteoarthritis knees are characterised by sclerotic bone that is less well mineralized. Arthritis Res Ther. 2009; 11(1): R11. Doi: 10.1186/ar2601

22. Taljanovic MS, Graham AR, Benjamin JB. Gmitro AF, Krupinski EA, Schwartz SA, Hunter TB, Resnick DL. Bone marrow edema pattern in advanced hip osteoarthritis: quantitative assessment with magnetic resonance imaging and correlation with clinical examination, radiographic findings and histopathology. Skeletal Radiol. 2008; 37(5): 423-31

23. Leydet-Quilici H, Le Corroller T, Bouvier C, Giorgi R, Argenson JN, Champsaur P, Pham T, de Paula AM, Lafforgue P. Advanced hip osteoarthritis: Magnetic Resonance Imaging aspects and histopathology correlations. Osteoarthritis Cartilage 2010; 18(11): 1429-35

24. Roemer FW, Guermazi A, Javaid MK, Lynch JA, Niu J, Zhang Y, Felson DT, Lewis CE, Tomer J, Nevitt MC, MOST Study Investigators. Change in MRI-detected subchondral bone marrow lesions is associated with cartilage loss: the MOST Study. A longitduninal multicentre study of knee osteoarthritis. Ann Rheum Dis 2009; 68(9): 1461-5

25. Carrino JA, Blum J, Parellada JA, Schweitzer ME, Morrison WB. MRI of bone marrow edema-like signal in the pathogenesis of subchondral cysts. Osteoarthritis Cartilage 2006; 14(10): 1081-5

26. Zhang D, Johnson LJ, Hsu H, Spector M. Cartilaginous Deposits in Subchondral Bone in Regions of Exposed Bone in Osteoarthritis of the Human Knee: Histomorphometric Study of PRG4 Distribution in Osteoarthritic Cartilage. Orthopaedic Research 2007; 25(7):873-83.

27. Campbell TM, Churchman SM, Gomez A, McGonagle D, Conaghan PG, Ponchel F, Jones E. Mesenchymal Stem Cell Alterations in Bone Marrow Lesions in Patients with Hip Osteoarthritis. Arthritis Rheumatism 2016; 68(7): 1648-1659

28. Jin K, Mao XO, Cottrell B, Schilling B, Xie L, Row RH, Sun Y, Peel A, Childs J, Gendeh G, Gibson BW, Greenberg DA. Proteomic and immunochemical characterization of a role for stathmin in adult neurogenesis. FASEB J. 2004; 18(2): 287-99

29. Liu H, Zhang R, Ko SY, Oyajobi BO, Papasian CJ, Deng HW, Zhang S, Zhao M. Microtubule assembly affects bone mass by regulating both osteoblast and

osteoclast functions: stathmin deficiency produces an osteopenic phenotype in mice. J Bone Miner Res. 2011; 26(9): 2052-67

30. Kim DS, Li KW, Boroujerdi A, Peter Yu Y, Zhou CY, Deng P, Park J, Zhnag X, Lee J, Corpe M, Sharp K, Steward O, Eroglu C, Barres B, Zaucke F, Xu ZC, Luo ZD. Thrombospondin-4 contributes to spinal sensitization and neuropathic pain states. J Neurosci 2012; 32(26): 8977-87

31. Pan B, Guo Y, Wu HE, Park J, Trinh VN, Luo ZD, Hogan QH. Thrombospondin-4 divergently regulates voltage-gated Ca2+ channel subtypes in sensory neurons after nerve injury. Pain 2016; 157(9): 2068-80

32. Foulkes T, Wood JN. Pain Genes. PLoS Genetics 2008; 4(7): e1000086

33. Swaminathan A, Delage H, Chatterjee S, Belgarbi-Dutron L, Cassel R, Martinez N, Cosquer B, Kumari S, Mongelard F, Lannes B, Cassel JC, Boutillier, Bouvet P, Kundu TK. Trnascriptional Coactivator and Chromatic Protein PC4 is Involved in Hippocampal Neurogenesis and Spatial Memory Extinction. J Biol Chem. 2016; 291(39): 20303-14

34. Sofat N. Analysing the role of endogenous matrix molecules in the development of osteoarthritis. International Journal of Experimental Pathology, 2009; 90:463-479

35. Hopwood B, Tsykin A, Findlay DM, Fazzalari NL. Microarray gene expression profiling of osteoarthritic bone suggests altered bone remodelling, WNT and transforming growth factor-β/bone morphogenic protein signalling. Arthritis Research & Therapy, 2007; 9:R100

36. Chou C, Wu C, Song I, Chuang H, Lu L, Chang J, Kuo S, Lee C, Wu J, Chen Y, Kraus VB, Lee MM. Genome-wide expression profiles of subchondral bone in osteoarthritis. Arthritis Research & Therapy 2013; 15:R190

37. Kusumbe AP, Ramasamy SK, Adams RH. Coupling of angiogenesis and osteogenesis by a specific vessel subtype in bone. Nature 2014; 507(7492): 323-8

38. Ramasamy SK, Kusumbe AP, Wang L, Adams RH. Endothelial Notch activity promotes angiogenesis and osteogenesis in bone. Nature 2014; 507(7492): 376-80

39. Ninomiya K, Miyamoto T, Imai J, Fujita N, Suzuki T, Iwasaki R, Yagi M, Watanabe S, Toyama Y, Suda T. Osteoclastic activity induces osteomodulin expression in osteoblasts. Biochemical and Biophysical Research Communications. 2007; 362(2): 460-466

40. Zhang Y-K, Huang Z-J, Liu S, Liu Y=P, Song AA, Song X-J. WNT signalling underlies the pathogenesis of neuropathic pain in rodents. Journal of Clinical Investigation 2013; 123(5): 2268-2286

41. Miller RE, Tran PB, Das R, Ghoreishi-Haack N, Ren D, Miller RJ, Malfait AM. CCR2 chemokine receptor signalling mediates pain in experimental osteoarthritis. Proc Natl Acad Sci USA 2012; 109(50): 20602-7

42. Walsh DA, McWilliams DF, Turley MJ, Dixon MR, Franses RE, Mapp PI, et al. Angiogenesis and nerve growth factor at the osteochondral junction in rheumatoid arthritis and osteoarthritis. Rheumatology (Oxford) 2010; 49: 1852-61.

43. Little CB, Baraj A, Burkhardt D, Smith SM, Fosang AJ, Werb Z, Shah M, Thompson EW. Matrix metalloproteinase 13-deficient mice are resistant to osteoarthritic cartilage erosion but not chondrocyte hypertrophy or osteophytes development. Arthritis Rheum 2009; 60(12): 3723-33.

44. Kofuji T, Fujiwara T, Sanada M, Mishima T, Akagawa K. HPC-1/syntaxin 1A and syntaxin 1B play distinct roles in neuronal survival. J Neurochem 2014; 130(4): 514-25

45. Vaudry D, Gonzalez BJ, Basille M, Fournier A, Vaudry H. Neurotrophic activity of pituitary adenylate cyclase-activating polypeptide on rat cerebellar cortex during development. PNAS 1999; 96: 9415-20

Table 1.

		Advanced OA	Mild OA	Tissue Control
Number*		72	12	10
Age Range Mean (SD)		51-88 69.1 (7.7)	49-79 62.2 (8.5)	21-88 56.2 (27.7)
Gender Female N (%)		55 (76.4%)	9 (75%)	9 (90%)
Body Mass Index Mean (SD)		32.5 (5.7)	28.8 (3.9)	N/A
WOMAC Pain Mean (SD)		59.4 (21.3)	30.9 (20.3)	N/A
WOMAC Stiffness Mean (SD)		62.8 (25.4)	33.0 (29.7)	N/A
WOMAC Function Mean (SD)		59.8 (20.6)	34.0 (24.3)	N/A
NRS Pain Mean (SD)		5.7 (2.3)	2.6 (2.4)	N/A
HADS Mean (SD)		12.6 (7.2)	9.6 (6.7)	N/A
MOAKS* N (%) BML	MOAKS = 0 MOAKS = 1 MOAKS = 2 MOAKS = 3	9 (14.1%) 52 (81.3%) 3 (4.6%) 0 (0%)	4 (57.1%) 3 (42.9%) 0 (0%) 0 (0%)	N/A
Synovitis/ Effusion	MOAKS = 0 MOAKS = 1 MOAKS = 2 MOAKS = 3	2 (3.1%) 28 (43.8%) 18 (28.1%) 16 (25%)	2 (28.6%) 2 (28.6%) 1 (14.2%) 2 (28.6%)	N/A
Cartilage damage	MOAKS = 0 MOAKS = 1 MOAKS = 2 MOAKS = 3	0 (0%) 16 (25%) 41 (64.1%) 7 (10.9%)	4 (57.1%) 3 (42.9%) 0 (0%) 0 (0%)	N/A
Clinical Management		Underwent knee replacement surgery	Medical management	Underwent other surgery

Table 2

Accession #	Symbol	Entity Name	↑↓	Abs FC	Log FC	P Value[a]	P Value[b]
NM_007029	STMN2	Stathmin 2	Up	19.30	4.27	3.67×10^{-6}	1.6×10^{-6}
NM_001163942	ABCB5	ATP-binding cassette, sub-family B (MDR/TAP), member 5	Up	12.11	3.60	2.06×10^{-6}	8.86×10^{-7}
NM_003248	THBS4	Thrombospondin 4	Up	11.53	3.53	1.31×10^{-4}	7.35×10^{-5}
NM_002427	MMP13	Matrix Metallopeptidase 13 (collagenase 3)	Up	11.18	3.48	2.78×10^{-5}	1.41×10^{-5}
NR_037585	C21orf37	Chromosome 21 open reading frame 37	Up	9.32	3.22	3.64×10^{-6}	1.65×10^{-6}
NM_001167890	EGFL6	EGF-like-domain, multiple 6	Up	9.07	3.18	2.69×10^{-5}	1.38×10^{-5}
NM_001856	COL16A1	Collagen, type XVI, alpha 1	Up	8.25	3.04	1.8×10^{-5}	9.08×10^{-6}
NM_020752	GPR158	G protein-coupled receptor 158	Up	8.21	3.04	1.13×10^{-4}	6.35×10^{-5}
NM_012093	AK5	Adenylate kinase 5	Up	8.01	3.00	5.77×10^{-6}	2.73×10^{-6}
NM_174858	AK5	Adenylate kinase 5	Up	8.01	3.00	3.33×10^{-5}	1.74×10^{-5}
NM_152565	ATP6V0D2	ATPase, H+ transporting, lysosomal 38kDa, V0 subunit d2	Up	7.89	2.98	4.11×10^{-6}	1.91×10^{-6}
	ALU2	Alu 2 Element	Up	7.44	2.89	1.32×10^{-6}	5.82×10^{-7}
NM_017594	DIRAS2	DIRAS family, GTP-binding RAS-like 2	Up	7.14	2.84	2.8×10^{-6}	1.29×10^{-6}
XR_245643	LOC101929504	Uncharacterized LOC101929504	Up	7.02	2.81	3.79×10^{-5}	2.02×10^{-5}
NM_021233	DNASE2B	Deoxyribonuclease II beta	Up	7.02	2.81	1.55×10^{-5}	7.86×10^{-6}
NM_014980	STXBP5L	Syntaxin binding protein 5-like	Up	6.72	2.75	2.68×10^{-6}	1.24×10^{-6}
NM_004789	LHX2	LIM homeobox 2	Up	6.71	2.75	7.61×10^{-5}	4.23×10^{-5}
NM_021144	PSIP1	PC4 and SFRS1 interacting protein 1	Up	6.57	2.72	3.62×10^{-6}	1.71×10^{-6}
NM_020864	NYAP2	Neuronal tyrosine-phosphorylated phosphoinositide-3-kinase adaptor 2	Up	6.48	2.70	2.53×10^{-5}	1.33×10^{-5}
NM_001332	CTNND2	Catenin (cadherin-associated protein), delta 2	Up	6.36	2.67	6.52×10^{-6}	3.19×10^{-6}
NM_032532	FNDC1	Fibronectin type III domain containing 1	Up	6.09	2.61	7×10^{-5}	3.91×10^{-5}
NM_001426	EN1	Engrailed homeobox 1	Up	5.75	2.52	1.21×10^{-6}	5.56×10^{-7}
NR_027054	MIR31HG	MIR31 host gene (non-protein coding)	Up	5.64	2.50	1.21×10^{-6}	1.03×10^{-4}
	XLOC_006820		Up	5.48	2.45	9.05×10^{-6}	4.6×10^{-6}
NM_014728	FRMPD4	FERM and PDZ domain containing 4	Up	5.34	2.42	3.09×10^{-5}	1.68×10^{-5}
TCONS_00014487	LOC101929450	Uncharacterized LOC101929450	Up	5.33	2.41	1.31×10^{-5}	6.78×10^{-6}
NM_022970	FGFR2	Fibroblast growth factor receptor 2	Up	5.30	2.41	9.69×10^{-6}	4.97×10^{-6}
NM_012152	LPAR3	Lysophosphatidic acid receptor 3	Up	5.27	2.40	3.65×10^{-5}	2×10^{-5}
NM_004370	COL12A1	Collagen, type XII, alpha 1	Up	5.27	2.40	1.32×10^{-6}	6.2×10^{-7}
BC043571	LOC613266	Uncharacterized LOC613266	Up	5.09	2.35	1.2×10^{-7}	5.25×10^{-8}
NM_000170	GLDC	Glycine dehydrogenase (decarboxylating)	Up	5.00	2.32	6.11×10^{-5}	3.46×10^{-5}
NM_031913	ESYT3	Extended synaptotagmin-like protein 3	Up	5.00	2.32	3.61×10^{-5}	1.99×10^{-5}
	ALU1	Alu 1 Element	Down	-5.02	-2.33	3.17×10^{-7}	1.44×10^{-7}
NM_025260	C6orf25	Chromosome 6 open reading frame 25	Down	-5.82	-2.54	5.35×10^{-6}	2.62×10^{-6}
NM_080429	AQP10	Aquaporin 10	Down	-6.92	-2.79	6.26×10^{-7}	2.62×10^{-6}
NM_005306	FFAR2	Free fatty acid receptor 2	Down	-7.29	-2.87	5.63×10^{-5}	3.06×10^{-5}
AB305916	TRBV28	T Cell Receptor Beta Variable 28	Down	-7.50	-2.91	3.35×10^{-6}	1.55×10^{-6}
NM_000517	HBA2	Hemoglobin, alpha 2	Down	-7.64	-2.93	7.61×10^{-7}	3.25×10^{-7}
	XLOC_014512		Down	-7.99	-3.00	2.74×10^{-7}	1.1×10^{-7}
NM_000517	HBA2	Hemoglobin, alpha 2	Down	-8.20	-3.04	5.59×10^{-7}	2.33×10^{-7}
NM_016509	CLEC1B	C-type lectin domain family 1, member B	Down	-8.24	-3.04	1.03×10^{-4}	2.33×10^{-7}
NM_002620	PF4V1	Platelet factor 4 variant 1	Down	-9.31	-3.22	2.34×10^{-6}	1.04×10^{-6}
NM_022468	MMP25	Matrix Metallopeptidase 25	Down	-9.33	-3.22	4.32×10^{-5}	2.28×10^{-5}
NR_120522	LOC102724484	Uncharacterized LOC102724484	Down	-10.04	-3.33	1.01×10^{-4}	5.6×10^{-5}
NM_001136503	SMIM24	Small integral membrane protein 24	Down	-10.29	-3.36	1.38×10^{-5}	6.73×10^{-6}
NM_030773	TUBB1	Tubulin, beta 1 class VI	Down	-12.37	-3.63	5.86×10^{-7}	2.34×10^{-7}
	HSJ1167H4		Down	-13.17	-3.72	3.71×10^{-6}	1.65×10^{-6}
NR_001552	TTTY16	Testis-specific transcript, Y-linked 16 (non-protein coding)	Down	-13.65	-3.77	6.28×10^{-5}	3.34×10^{-5}
NR_047499	LINC00570	Long intergenic non-protein coding RNA 570	Down	-14.00	-3.81	1.03×10^{-4}	8.67×10^{-5}
NM_144673	CMTM2	CKLF-like MARVEL transmembrane domain containing 2	Down	-14.25	-3.83	2.71×10^{-5}	1.36×10^{-5}
NM_001557	CXCR2	Chemokine (C-X-C motif) receptor 2	Down	-14.93	-3.90	9.27×10^{-6}	4.34×10^{-6}
NM_000519	HBD	Hemoglobin, delta	Down	-15.75	-3.98	7.89×10^{-8}	2.74×10^{-8}
NM_002100	GYPB	Glycophorin B (MNS blood group)	Down	-16.15	-4.01	1.03×10^{-4}	1.43×10^{-4}
XM_005261527	SEC14L3	SEC14-like 3 (S. cerevisiae)	Down	-16.65	-4.06	2.98×10^{-5}	1.5×10^{-5}
AK128128	FLJ46249		Down	-16.90	-4.08	6.19×10^{-5}	3.27×10^{-5}
NM_016509	CLEC1B	C-type lectin domain family 1, member B	Down	-17.06	-4.09	1.34×10^{-5}	6.39×10^{-6}
NM_016509	CLEC1B	C-type lectin domain family 1, member B	Down	-17.67	-4.14	4.83×10^{-6}	2.15×10^{-6}
NM_002049	GATA1	GATA binding protein 1 (globin transcription factor 1)	Down	-19.55	-4.29	7.87×10^{-5}	4.21×10^{-5}
NM_005764	PDZK1IP1	PDZK1 interacting protein 1	Down	-20.36	-4.35	7.59×10^{-6}	3.47×10^{-6}
NM_006163	NFE2	Nuclear factor, erythroid 2	Down	-22.54	-4.49	3.22×10^{-5}	1.62×10^{-5}
	XLOC_013489		Down	-23.69	-4.57	2.85×10^{-5}	1.42×10^{-5}
NM_002619	PF4	Platelet factor 4	Down	-31.42	-4.97	1.26×10^{-7}	4.32×10^{-8}
	XLOC_000346		Down	-31.94	-5.00	1.26×10^{-7}	2.56×10^{-5}
NM_000032	ALAS2	Aminolevulinate, delta-, synthase 2	Down	-33.49	-5.07	1.93×10^{-5}	9.3×10^{-6}
NM_005980	S100P	S100 calcium binding protein P	Down	-33.56	-5.07	1.11×10^{-4}	6.06×10^{-5}
NM_005331	HBQ1	Hemoglobin, theta 1	Down	-34.07	-5.09	3.58×10^{-6}	1.53×10^{-6}
NM_002704	PPBP	Pro-platelet basic protein (chemokine (C-X-C motif) ligand 7)	Down	-39.94	-5.32	4.11×10^{-8}	1.3×10^{-8}
NM_000517	HBA2	Hemoglobin, alpha 2	Down	-41.07	-5.36	2.47×10^{-7}	8.77×10^{-8}
NM_001003938	HBM	Hemoglobin, mu	Down	-45.11	-5.50	7.66×10^{-5}	4.05×10^{-5}
NM_018437	HEMGN	Hemogen	Down	-53.12	-5.73	1.89×10^{-6}	7.66×10^{-7}
NM_005621	S100A12	S100 calcium binding protein A12	Down	-56.95	-5.83	7.25×10^{-5}	3.81×10^{-5}
NM_005621	S100A12	S100 calcium binding protein A12	Down	-58.82	-5.88	4.6×10^{-5}	2.34×10^{-5}
NM_000559	HBG1	Hemoglobin, gamma A	Down	-88.82	-6.47	1.94×10^{-6}	7.82×10^{-7}

Accession #: Accession Number. Symbol: Entity Symbol. ↑↓: Regulation. Abs FC: Absolute Fold Change. Log FC: Log transformed Fold Change. P Value[a]: Adjusted Student T-test P value for microarray corrected for multiple testing by the Bonferroni FWER method. P Value[b]: Adjusted Moderated T-test P value for microarray corrected for multiple testing by the Bonferroni FWER method.

* Supplementary table of whole dataset provided in supplementary section.

Figure 1

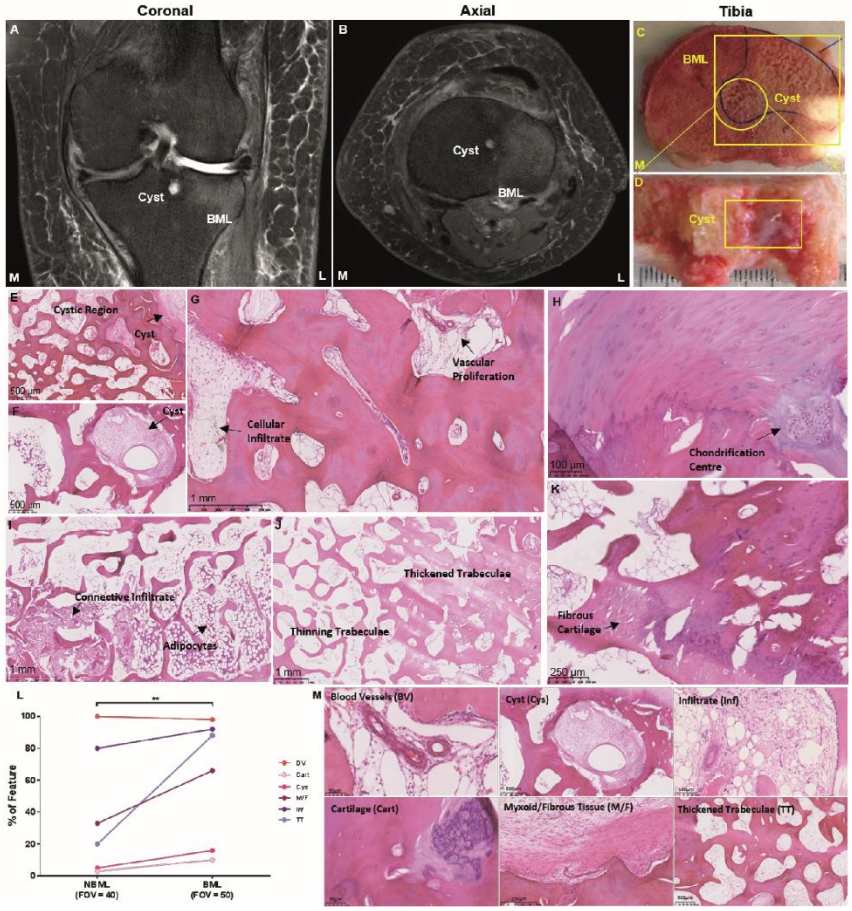
Coronal
Axial
Tibia
A
Cyst
BML
M
L
B
Cyst
BML
M
L
C
BML
Cyst
M
D
Cyst
E
Cystic Region
Cyst
500 µm
F
Cyst
500 µm
G
Vascular Proliferation
Cellular Infiltrate
1 mm
H
Chondrification Centre
100 µm
I
Connective Infiltrate
Adipocytes
1 mm
J
Thickened Trabeculae
Thinning Trabeculae
1 mm
K
Fibrous Cartilage
250 µm
L
**
% of Feature
100
80
60
40
20
0
NBML (FOV = 40)
BML (FOV = 50)
OV
Cart
Cyst
M/F
INF
TT
M
Blood Vessels (BV)
Cyst (Cys)
Infiltrate (Inf)
Cartilage (Cart)
Myxoid/Fibrous Tissue (M/F)
Thickened Trabeculae (TT)

Figure 2.

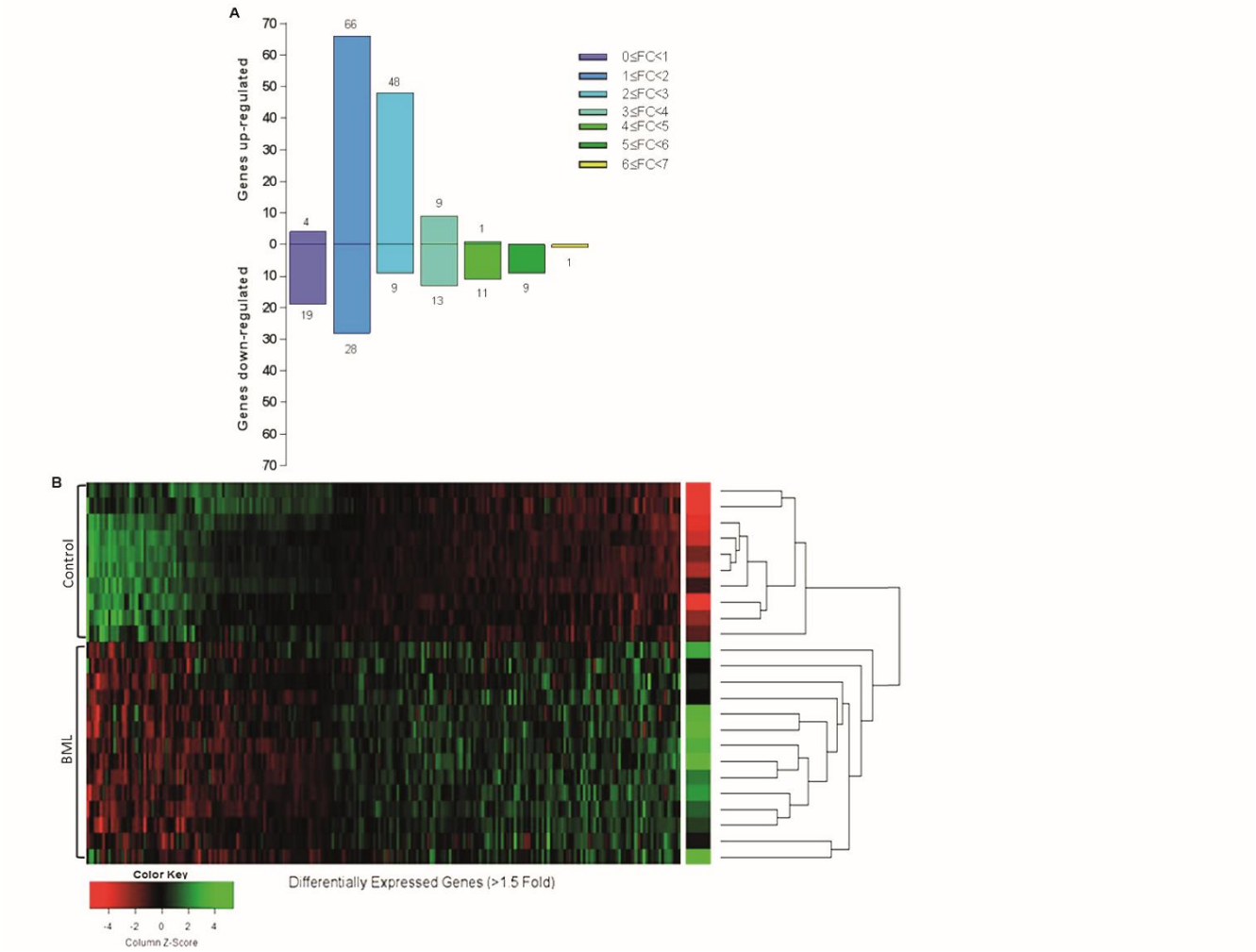
A
Genes up-regulated
Genes down-regulated
0≤FC<1
1≤FC<2
2≤FC<3
3≤FC<4
4≤FC<5
5≤FC<6
6≤FC<7
4
66
48
9
1
1
19
28
9
13
11
9
B
Control
BML
Color Key
-4
-2
0
2
4
Column Z-Score
Differentially Expressed Genes (>1.5 Fold)

Figure 3.

A.

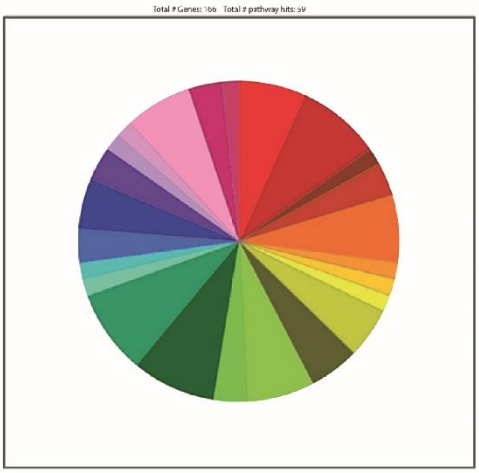

- Alzheimer disease-presenilin pathway
- Angiogenesis
- Apoptosis signalling pathway
- B cell activation
- CCKR signalling map
- Cadherin signalling pathway
- Cytoskeletal regulation by Rho GTP ase
- De novo purine biosynthesis
- EGF-receptor signalling
- FGF signalling pathway
- Gonadotrophin releasing hormone receptor pathway
- Huntington disease
- Inflammation mediated by chemokine and cytokine signalling pathway
- Integrin signalling pathway
- Interleukin signalling pathway
- Nicotinic acetylcholine receptor signalling pathway
- Notch signalling pathway
- PDGF signalling pathway
- Plasminogen activating cascade
- T cell activation
- TGF-beta signalling pathway
- VEGF signalling pathway
- Wnt signalling pathway
- P39 MAPK pathway

B.

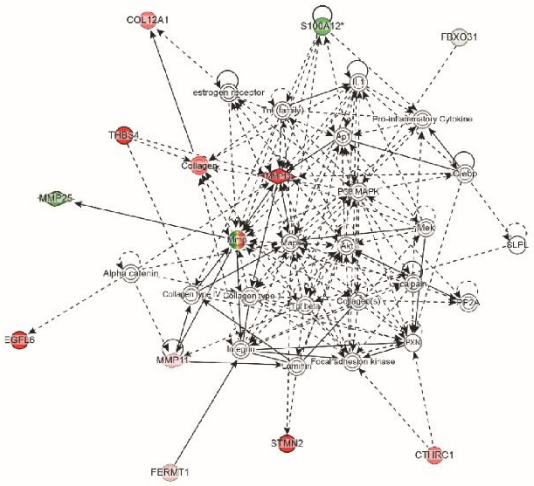

Molecules in Network	Focus Molecules
Akt, Alpha catenin, Ap1, C/ebp, calpain, ↑COL12A1, Collagen, Collagen type 1, Collagen type IV, Collagen(s), ↑CTHRC1, ↑EGFL6, estrogen receptor, ↓FBXO31, ↑FERMT1, Focal adhesion kinase, IL1, Integrin, Laminin, Mapk, Mek, MMP, ↑MMP11, ↑MMP13, ↓MMP25, P38 MAPK, PP2A, Pro-inflammatory Cytokine, ↓PXN, ↓S100A12, ↓SLPL, ↑STMN2, Tgf beta, ↑THBS4, Tnf (family)	↑COL12A1, ↑CTHRC1, ↑EGFL6, ↓FBXO3, ↑FFRMT1, ↑MMP11, ↑MMP13, ↓MMP25, ↓PXN, ↓S100A12, ↓SLPL, ↑STMN2, ↑THBS4

Figure 4.

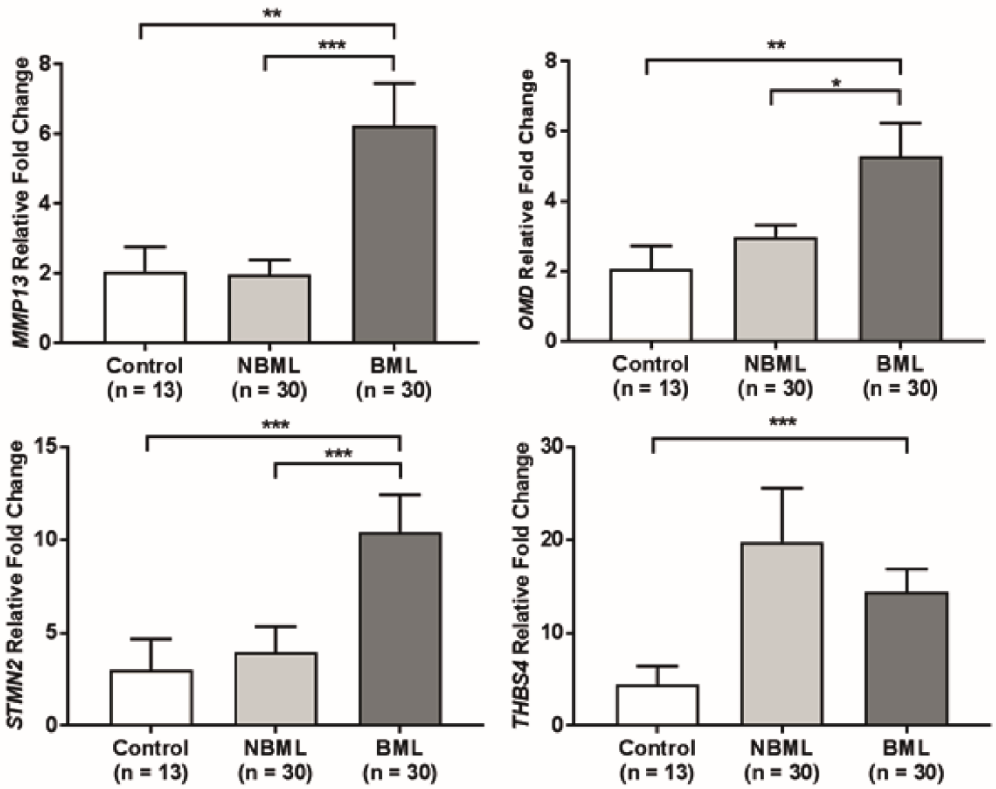
MMP13 Relative Fold Change
OMD Relative Fold Change
STMN2 Relative Fold Change
THBS4 Relative Fold Change
Control (n = 13)
NBML (n = 30)
BML (n = 30)
**
***
*

Supplementary Figure 1.

A.

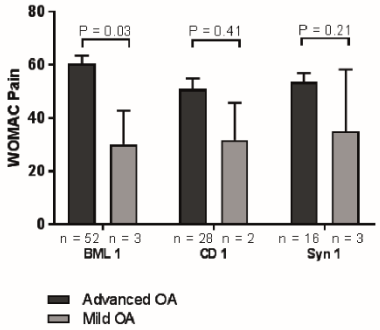

B.

MOAKS (n=62)	WOMAC pain correlation r value	P value
Bone Marrow Lesion	-0.145	0.023
Cartilage Damage	-0.012	0.85
Synovitis	0.053	0.408

C.

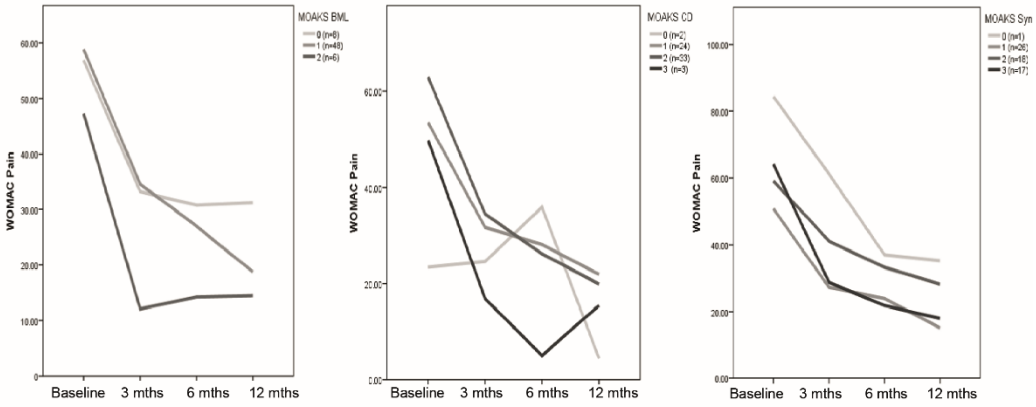

Supplementary Figure 2.

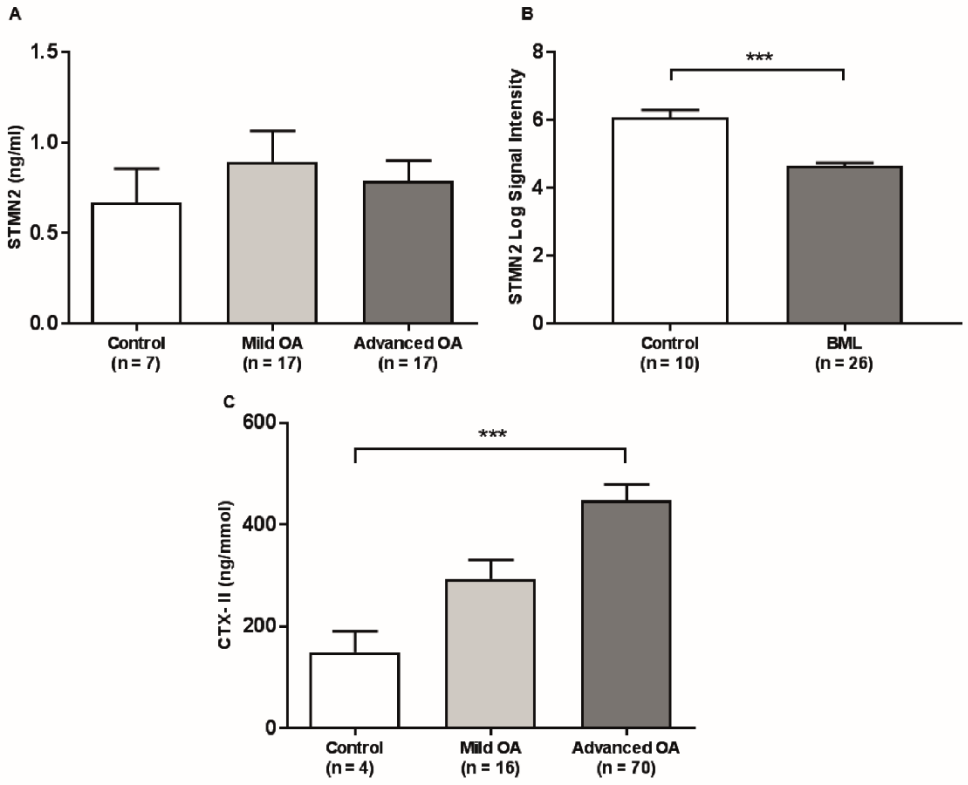

Supplementary methods

Study consent, control participants and exclusion criteria.

Subjects were consented by a research associate independent of the treating physicians, for knee MRI of the target joint and waste joint tissue collection at TKR. Participants without knee OA were recruited as control subjects aged 35-90 years. Exclusion was made for other diagnoses e.g. rheumatoid arthritis, systemic lupus erythematosus, fibromyalgia, pregnancy, regular use of bisphosphonates, steroids or hormone replacement therapy within the last 6 months, history of clinically-diagnosed depression or anxiety and other recent surgery.

Magnetic Resonance Imaging

A Philips 3T MRI scanner acquired images from participants within six weeks before TKR to ensure the visualisation of structural changes, including BML, synovitis and cartilage damage. Multimodal MRI scans lasted 30 minutes and included scout images, T2-weighted imaging for lesion detection, 3D T1-weighted imaging for delineating knee structures, with T2 fat suppression for BML visualisation. All data were acquired using protocols that complied with scanner safety procedures and full CE-marking in place, with adherence to all contra-indications to MRI scanning. A dedicated 8 channel knee coil was used. Pulse sequences were sagittal, coronal and axial intermediate-weighted images with TE 30 ms, TR 500 ms and SPAIR fat-saturation and sagittal T1-weighted with TE 15 ms, TR 600 ms. Radiographic changes were evaluated independently for anonymised scans using the validated MRI Knee Osteoarthritis Score (MOAKS) (14) by two consultant radiologists (VE and CH) and consensus scores reached. For both BML size, cartilage damage and synovitis, a mean of the consensus scores for all of the regions was calculated for each participant.

Microarray and QPCR methods

The aim of the transcriptomic analysis was to select specific sites of OA BML pathology for analysis. As the largest number of significant lesions were observed in the tibial compartment, this site was selected for OA BML evaluation from consecutively enrolled participants. The control bone comparator group were distinct participants who were undergoing surgery following trauma, e.g. amputation, fracture correction or trochleoplasty, with no clinical or radiographic arthritis.

Region of interest localisation and RNA isolation. MR images were viewed as DICOM files using an image processing and analysis software (ImageJ, NIH, Wayne Rasband, 1997). Axial image dimensions were set as: pixel width 0.25mm and pixel height: 0.2mm on ImageJ then scaled at 160mm x 160mm in line with the field of view. A 2cm x 2cm grid was drawn over the axial images and the MOAKS scoring was used to confirm the location of the lesions. The tibial plateau was placed over a grid of 2cm x 2cm with 1mm increments. This was used in line with the scaled axial images to measure and locate the BMLs. Once the lesions were located a region of bone of approximate equivalence that was macroscopically normal in appearance was taken approximately ≥5cm lateral to the lesion to use as the non-BML (NBML) control sample and both regions were dissected using a hack saw. The samples were washed in PBS and divided equally into two: one part stored at -80ºC for gene expression studies and the other fixed in 10% (v/v) natural buffered formalin (VWR, Leicestershire, UK) for histological analysis. A region of bone that was macroscopically normal in appearance was taken from the tissue control comparator bone and was dissected of all soft tissue and cartilage, washed in PBS and stored for future use at -80ºC.

RNA isolation and Whole Transcriptomic Analysis. Total RNA was isolated from approx.. 200mg of bone tissue using Qiazol and the RNeasy Mini Kit (Qiagen, Crawley, UK) according to manufacturer's instructions (15). Total RNA was measured via spectrophotometry using a Nanodrop 1000 (Thermo Scientific, Hertfordshire, UK). Integrity and purity of the RNA was assessed via microfluidic electrophoretic technology using an Agilent 2100 bioanalyzer (RIN 6.5-8) (Agilent Technologies, Santa Clara, CA, US). Total RNA (200ng) isolated from bone tissue, from 10 healthy controls and 14 OA patients with extensive BMLs, were used for one round of cRNA synthesis and amplification using a LowInput QuickAmp Labelling Kit with the addition of positive control transcripts for monitoring the Agilent One Color Gene Expression microarray workflow using an RNA Spike In Kit – One Color (Agilent Technologies, Santa Clara, CA, USA). The Cyanine 3-labeled cRNA was quantified via spectrophotometry using a Nanodrop 1000 and purified using the RNeasy Mini Kit. The linearly amplified Cyanine 3-labeled cRNA samples (600ng) were hybridized to Agilent whole human genome 60k microarray chips and washed using buffers from the Gene Expression Wash Pack (Agilent Technologies, USA). Microarray chips were scanned using an Agilent SureScan High-Resolution DNA Microarray Scanner and Feature extraction performed using the Feature Extraction Software (version 11.5.1.1). Array signal intensities were analysed by the Agilent Gene-Spring GX software (version 11.5). The dataset was normalized by quantile normalization. Significant differentially expressed entities between bone samples from healthy controls and OA patients were selected using a union of a student's and moderated t-test corrected for multiple comparisons with the Bonferroni FWER correction ($P < 0.05$). Probes with a threshold of ≥1.5 fold-change were selected and these entities were additionally analysed by the hierarchical clustering method, with a Pearson

correlation coefficient algorithm and an average linkage method. Significant differentially expressed gene IDs were uploaded onto PANTHER pathway analysis (PANTHER Classification Systems 10.0; www.pantherdb.org) for functional classification. The online resource includes functional annotations from the GO Phylogenetic Annotation project for the biological interpretation of large-scale experimental datasets (17). The gene IDs were also loaded into Ingenuity Pathway Analysis (Ingenuity Systems; www.ingenuity.com) to identify functional annotations and predict biological interactions. The biological interaction scores were defined by the IPA statistical algorithm: based on the z-score and P-value, which were calculated by the IPA regulation z-score algorithm and the Fischer's exact test. A positive or negative z-score of more than 1.5 or less than 1.5, and P-value less than 0.05 (-log10 ≥1.5) indicates a significant biological function and predicts that the biological process or condition is leaning towards an increase (z-score ≥1.5) or decrease (z-score ≤ -1.5). P values were corrected for multiple comparisons with the Benjamini-Hochberg test.

Quantitative Reverse-Transcription PCR Validation. To validate the microarray analysis quantitative polymerase chain reaction (qPCR) was performed for the most significantly upregulated genes. The genes of interest (GOI) were identified for verification on the basis of significant fold-change (≥1.5; P <0.05) between the OA BML, OA NBML and control groups. Expression of matrix metalloproteinase 13 (*MMP13*), stathmin 2 (*STMN2*) and thrombospondin 4 (*THBS4*) was analysed using osteomodulin (*OMD*) a bone turnover gene expressed in osteoblasts and osteoclasts as a positive tissue control. To select a fixed group of reference genes the geNorm reference gene selection kit (PrimerDesign, Southampton, UK) was used. The kit incorporates 12 of the most notably cited candidate reference genes for which qPCR was used to measure expression in disease and non-disease tissue. The geNorm

Biogazelle qbase PLUS software was used to analyse the data resulting in a list of the most optimal reference genes for accurate normalisation dependent on the stability of their expression. ATP Synthase, H+ Transporting, Mitochondrial F1 (*ATP5B)*, Cytochrome C1 (*CYC1*), Eukaryotic Translation Initiation Factor 4A2 (*EIF4A2*) and Succinate Dehydrogenase Complex Flavoprotein Subunit A (*SDHA*) were selected as endogenous reference genes. BML regions were analysed in 30 BML and 30 NBML matched bone tissue samples using 13 healthy control bone samples for the control comparator group. Total RNA from each region was reverse transcribed into 1µg of cDNA using Superscript II reverse transcriptase (Invitrogen, Paisley, UK). RNA samples below 100ng/µl were extracted, pooled and concentrated using a SpeedVac™ Concentrator (Savant SPD131DDA, Thermo Fisher Scientific, MA, USA). The qPCR was performed using GoTaq SYBR Green florescence system (Promega, Southampton, UK) according to the manufacturer's instructions. The qPCR reactions were performed on the Bio-Rad CFX96 or CFX384 Real-Time PCR Detection System (Bio-Rad Laboratories, Hertfordshire, UK) and the fluorescent signal intensity was analysed by CFX Manager Software (Bio-Rad Laboratories, Hertfordshire, UK). Two-tailed unpaired Mann Whitney U statistical testing was performed to evaluate statistically significant differences in gene expression levels between groups.

Primer sequences used are summarised below

Gene Symbol	Accession Number	Sequence Length	Sense Primer	Anti-sense Primer
GENES OF INTEREST				
MMP13	NM_002427	2735	ATGAAGACCCCAACCCTAAACA	CGGAGACTGGTAATGGCATCA
STMN2	NM_001199214	2314	AAGCCCCACGAACTTTAG	CGTGTTCCCTCTTCTCTG
THBS4	NM_003248	3233	AGAGAGGCAGGGGGATGTG	TTCTTCGTCGGGGTAACTGTC
POSITIVE TISSUE CONTROL				
OMD	NM_005014	2542	CAGTAACAGATTAGAATCAATGCC	GACATTCTTAGAGTATGAAGTTTTGGA

Histology

Four patient samples were consecutively selected and specimens were fixed in 10% (v/v) neutral buffered formalin for 24 hours then decalcified using formic acid containing 40% (v/v) formalin. Specimens were placed in the decalcification solution at 20 times the tissue volume for up to 14 days at room temperature. Samples were dehydrated in graded alcohol series and paraffin embedded before being sectioned using a microtome at 5µm (Leica RM2255, Milton Keynes, UK). Sections were stained with haematoxylin and eosin (H&E) (Leica, Milton Keynes, UK). Slides were scanned using a NanoZoomer 2.0-RS Digital Scanner (Hamamatsu, Hertfordshire, UK) and visualised using the NanoZoomer Digital Pathology v2.0 software (Hamamatsu, Hertfordshire, UK). The scans were used to analyse 50 BML, 10 Cyst and 40 non-BML (NBML) fields of view (FOV) for the presence of blood vessels (BV), cartilage within the bone compartment (Cart), cysts (Cys), myxoid/fibrous tissue (M/F), cellular infiltrate (Inf) and trabecular thickening (TT). A percentage for the presence of each histological feature was determined for each group. Significance was tested between the two groups using the Friedman test ($P<0.05$).

Enzyme-Linked ImmunoSorbent Assay

CTX- II ELISA. Detection of C-terminal telopeptides of type II collagen cleavage products was conducted using the Urine Cartilaps (CTX-II) EIA (Immunodiagnostic Systems) as previously described (18). Urine samples collected at the first visit were sampled for type II collagen cleavage products. Matched urine samples were tested for creatinine for normalisation. Absorbance of each well was read at 450 nm.

STMN2 ELISA. Quantitative determination of STMN2 in human serum from 17 end-stage OA, 17 early OA and 7 healthy controls was performed using the US Biological STMN2 BioAssay ELISA Kit for human samples (United States Biological, Salem, MA, USA) adhering to manufacturer instructions. The ELISA kit employs the competitive enzyme-linked immunoassay technique with a colorimetric detection method measured at 450nm on a Molecular Devices Spectra Max 340 microplate reader (Molecular Devices, Berkshire, UK). The intensity of the absorbance is inversely proportional to the concentration of STMN2 present within the serum sample or standards. A standard curve was plotted relating the absorbance (OD) to the concentration of the standards (ng/ml). The STMN2 concentration in each sample was interpolated from the standard curve and results plotted on GraphPad Prism 7.01 (GraphPad Prism, San Diego, CA, USA). Kruskal-Wallis statistical testing was performed to evaluate statistically significant differences in STMN2 levels between groups

Quantitative Western Blot Analysis

For the quantitative detection of STMN2 within the bone samples 26 BML bone and 10 control bone samples were homogenised in RIPA buffer with protein inhibitors (PMSF, aprotinin and 1mM sodium orthovanadate) using a Fast Prep homogeniser for 3 bursts at 20 seconds, sonicated 3 x 5 seconds at 60% amplitude and clarified by centrifugation for 10 minutes. Appropriate dilutions of the supernatant were used in a Bradford protein assay (Sigma – Aldrich, MO, USA). Samples were denatured in 5X sample buffer at 99ºC and 50µg of protein loaded and run on SDS-Tris gels. All gels were run using the Bio-Rad Mini PROTEAN Tetra electrophoretic tank system run at a constant current (60mA) for 1-2 hours. The Gels were transferred onto PVDF using

the Bio-Rad Mini-PROTEAN transfer system at a constant current (300mA) for 1 hour (Bio-Rad Laboratories, Hertfordshire, UK). Membranes were incubated with Odyssey PBS blocking buffer (1:1 dilution) (LI-COR Biosciences, NE, USA) prior to incubation with rabbit polyclonal antibody directed against STMN2 (1:500, Thermo Fischer Scientific, MA, USA, #720178) and mouse monoclonal anti-β-actin (1:2000, Sigma-Aldrich MO, USA, #A2228) made up in LiCor blocking buffer plus 0.2% (v/v) Tween®20 overnight at 4°C. Goat anti-rabbit IgG (H+L) Alexa Fluor® 700 and donkey anti-mouse IgG Alexa Fluor® 790 (1:10,000, Thermo Fischer Scientific, MA, USA, #A21038, #A11371) made up in LiCor blocking buffer plus 0.2% (v/v) Tween® 20 were applied for 60 minutes at room temperature prior to washing with PBS + 0.1% (v/v) Tween®20. Visualisation and quantification of the blots were carried out using the LI-COR Odyssey® scanner and software (LI-COR Biosciences). Normalised signal intensity values were obtained by subtracting the background and dividing the protein of interest (STMN2) densities by the relative normalising control (β-actin) values. The values were log transformed and evaluated for statistical significance using a two-tailed unpaired t-test.

Supplementary Table 1.

Accession #	Symbol	Entity Name	↑↓	Abs FC	Log FC	P Value[a]	P Value[b]
NM_007029	STMN2	Stathmin 2	Up	19.30	4.27	3.67×10^{-6}	1.6×10^{-6}
NM_001163942	ABCB5	ATP-binding cassette, sub-family B (MDR/TAP), member 5	Up	12.11	3.60	2.06×10^{-6}	8.86×10^{-7}
NM_003248	THBS4	Thrombospondin 4	Up	11.53	3.53	1.31×10^{-4}	7.35×10^{-5}
NM_002427	MMP13	Matrix Metallopeptidase 13 (collagenase 3)	Up	11.18	3.48	2.78×10^{-5}	1.41×10^{-5}
NR_037585	C21orf37	Chromosome 21 open reading frame 37	Up	9.32	3.22	3.64×10^{-6}	1.65×10^{-6}
NM_001167890	EGFL6	EGF-like-domain, multiple 6	Up	9.07	3.18	2.69×10^{-5}	1.38×10^{-5}
NM_001856	COL16A1	Collagen, type XVI, alpha 1	Up	8.25	3.04	1.8×10^{-5}	9.08×10^{-6}
NM_020752	GPR158	G protein-coupled receptor 158	Up	8.21	3.04	1.13×10^{-4}	6.35×10^{-5}
NM_012093	AK5	Adenylate kinase 5	Up	8.01	3.00	5.77×10^{-6}	2.73×10^{-6}
NM_174858	AK5	Adenylate kinase 5	Up	8.01	3.00	3.33×10^{-5}	1.74×10^{-5}
NM_152565	ATP6V0D2	ATPase, H+ transporting, lysosomal 38kDa, V0 subunit d2	Up	7.89	2.98	4.11×10^{-6}	1.91×10^{-6}
	ALU2	Alu 2 Element	Up	7.44	2.89	1.32×10^{-6}	5.82×10^{-7}
NM_017594	DIRAS2	DIRAS family, GTP-binding RAS-like 2	Up	7.14	2.84	2.8×10^{-6}	1.29×10^{-6}
XR_245643	LOC101929504	Uncharacterized LOC101929504	Up	7.02	2.81	3.79×10^{-5}	2.02×10^{-5}
NM_021233	DNASE2B	Deoxyribonuclease II beta	Up	7.02	2.81	1.55×10^{-5}	7.86×10^{-6}
NM_014980	STXBP5L	Syntaxin binding protein 5-like	Up	6.72	2.75	2.68×10^{-6}	1.24×10^{-6}
NM_004789	LHX2	LIM homeobox 2	Up	6.71	2.75	7.61×10^{-5}	4.23×10^{-5}
NM_021144	PSIP1	PC4 and SFRS1 interacting protein 1	Up	6.57	2.72	3.62×10^{-6}	1.71×10^{-6}
NM_020864	NYAP2	Neuronal tyrosine-phosphorylated phosphoinositide-3-kinase adaptor 2	Up	6.48	2.70	2.53×10^{-5}	1.33×10^{-5}
NM_001332	CTNND2	Catenin (cadherin-associated protein), delta 2	Up	6.36	2.67	6.52×10^{-6}	3.19×10^{-6}
NM_032532	FNDC1	Fibronectin type III domain containing 1	Up	6.09	2.61	7×10^{-5}	3.91×10^{-5}
NM_001426	EN1	Engrailed homeobox 1	Up	5.75	2.52	1.21×10^{-6}	5.56×10^{-7}
NR_027054	MIR31HG	MIR31 host gene (non-protein coding)	Up	5.64	2.50	1.21×10^{-6}	1.03×10^{-4}
	XLOC_006820		Up	5.48	2.45	9.05×10^{-6}	4.6×10^{-6}
NM_014728	FRMPD4	FERM and PDZ domain containing 4	Up	5.34	2.42	3.09×10^{-5}	1.68×10^{-5}
TCONS_00014487	LOC101929450	Uncharacterized LOC101929450	Up	5.33	2.41	1.31×10^{-5}	6.78×10^{-6}
NM_022970	FGFR2	Fibroblast growth factor receptor 2	Up	5.30	2.41	9.69×10^{-6}	4.97×10^{-6}
NM_012152	LPAR3	Lysophosphatidic acid receptor 3	Up	5.27	2.40	3.65×10^{-5}	2×10^{-5}
NM_004370	COL12A1	Collagen, type XII, alpha 1	Up	5.27	2.40	1.32×10^{-6}	6.2×10^{-7}
BC043571	LOC613266	Uncharacterized LOC613266	Up	5.09	2.35	1.2×10^{-7}	5.25×10^{-8}
NM_000170	GLDC	Glycine dehydrogenase (decarboxylating)	Up	5.00	2.32	6.11×10^{-5}	3.46×10^{-5}
NM_031913	ESYT3	Extended synaptotagmin-like protein 3	Up	5.00	2.32	3.61×10^{-5}	1.99×10^{-5}
NM_012194	KIAA1549L	KIAA1549-like	Up	4.90	2.29	1.69×10^{-5}	9.02×10^{-6}
NM_001287763	NSG1	Neuron specific gene family member 1	Up	4.84	2.27	1.3×10^{-4}	7.67×10^{-5}
NM_207338	LCTL	Lactase-like	Up	4.78	2.26	7.91×10^{-6}	4.10×10^{-6}

NM_001004342	TRIM67	Tripartite motif containing 67	Up	4.78	2.26	3.19×10^{-5}	1.76×10^{-5}
NM_006240	PPEF1	Protein phosphatase, EF-hand calcium binding domain 1	Up	4.76	2.25	1.01×10^{-4}	1.01×10^{-4}
NM_001935	DPP4	Dipeptidyl-peptidase 4	Up	4.76	2.25	9.81×10^{-6}	5.13×10^{-6}
NM_025061	LRRC8E	Leucine rich repeat containing 8 family, member E	Up	4.73	2.24	2.23×10^{-5}	1.21×10^{-5}
NM_024337	IRX1	Iroquois homeobox 1	Up	4.68	2.23	1.18×10^{-5}	6.23×10^{-6}
NM_138455	CTHRC1	Collagen triple helix repeat containing 1	Up	4.65	2.22	4.4×10^{-5}	2.47×10^{-5}
AJ295982			Up	4.62	2.21	7.65×10^{-6}	3.99×10^{-6}
NM_138461	TM4SF19	Transmembrane 4 L six family member 19	Up	4.59	2.20	1.08×10^{-4}	6.33×10^{-5}
NM_031913	ESYT3	Extended synaptotagmin-like protein 3	Up	4.50	2.17	1.1×10^{-4}	6.48×10^{-5}
NM_001145715	KPNA7	Karyopherin alpha 7 (importin alpha 8)	Up	4.48	2.16	8.21×10^{-6}	4.32×10^{-6}
NM_025074	FRAS1	Fraser syndrome 1	Up	4.46	2.16	1.31×10^{-5}	7.06×10^{-6}
NM_001742	CALCR	Calcitonin receptor	Up	4.44	2.15	1.43×10^{-4}	8.54×10^{-5}
AK096928			Up	4.42	2.15	6.46×10^{-5}	3.73×10^{-5}
NM_001129742	CALHM3	Calcium homeostasis modulator 3	Up	4.42	2.14	1.04×10^{-4}	1.04×10^{-4}
NM_001146188	TOX3	TOX high mobility group box family member 3	Up	4.36	2.12	1.24×10^{-4}	1.24×10^{-4}
NM_004460	FAP	Fibroblast activation protein, alpha	Up	4.33	2.11	5.15×10^{-5}	2.95×10^{-5}
			Up	4.24	2.08	4.49×10^{-8}	2.12×10^{-8}
NM_004717	DGKI	Diacylglycerol kinase, iota	Up	4.20	2.07	2.38×10^{-5}	1.32×10^{-5}
NM_002839	PTPRD	Protein tyrosine phosphatase, receptor type, D	Up	4.18	2.06	1.36×10^{-4}	8.19×10^{-5}
NM_020962	IGDCC4	Immunoglobulin superfamily, DCC subclass, member 4	Up	4.14	2.05	8.49×10^{-5}	5.29×10^{-5}
NM_031302	GLT8D2	Glycosyltransferase 8 domain containing 2	Up	4.10	2.04	7.25×10^{-5}	4.26×10^{-5}
NM_001007237	IGSF3	Immunoglobulin superfamily, member 3	Up	4.09	2.03	1.38×10^{-5}	7.60×10^{-6}
NM_207645	C11orf87	Chromosome 11 open reading frame 87	Up	4.09	2.03	4.09×10^{-5}	2.34×10^{-5}
NM_194312	ESPNL	Espin-like	Up	3.99	2.00	9.85×10^{-5}	5.89×10^{-5}
NM_001040708	HEY1	Hes-related family bHLH transcription factor with YRPW motif 1	Up	3.97	1.99	2.92×10^{-5}	1.66×10^{-5}
NM_030788	DCSTAMP	Dendrocyte expressed seven transmembrane protein	Up	3.92	1.97	2.79×10^{-5}	1.59×10^{-5}
NM_014568	GALNT5	Polypeptide N-acetylgalactosaminyltransferase 5	Up	3.91	1.97	6.38×10^{-5}	3.76×10^{-5}
NR_110267	LOC101927619	Uncharacterized LOC101927619	Up	3.89	1.96	4.22×10^{-5}	2.45×10^{-5}
NM_015265	SATB2	SATB homeobox 2	Up	3.84	1.94	2.65×10^{-5}	1.52×10^{-5}
NM_000165	GJA1	Gap junction protein, alpha 1, 43kDa	Up	3.81	1.93	1.98×10^{-7}	1.01×10^{-7}
NM_178833	SLC9B2	Solute carrier family 9, subfamily B, member 2	Up	3.81	1.93	6.92×10^{-5}	4.11×10^{-5}
NM_052909	PLEKHG4B	Pleckstrin homology domain containing, family G	Up	3.76	1.91	1.09×10^{-4}	1.09×10^{-4}
	LINC00673	Long intergenic non-protein coding RNA 673	Up	3.72	1.90	1.92×10^{-6}	1.03×10^{-6}
NM_001123366	HMSD	Histocompatibility (minor) serpin domain containing	Up	3.67	1.88	1.11×10^{-4}	1.11×10^{-4}
NM_003485	GPR68	G protein-coupled receptor 68	Up	3.64	1.86	1.19×10^{-4}	7.34×10^{-5}
			Up	3.53	1.82	9.90×10^{-5}	9.90×10^{-5}

NM_001164737	CALCR	Calcitonin receptor	Up	3.51	1.81	6.34×10^{-5}	3.83×10^{-5}
NM_003619	PRSS12	Protease, serine, 12 (neurotrypsin, motopsin)	Up	3.50	1.81	4.07×10^{-5}	2.42×10^{-5}
NM_003247	THBS2	Thrombospondin 2	Up	3.49	1.80	1.05×10^{-4}	1.05×10^{-4}
NM_001258248	SP6	Sp6 transcription factor	Up	3.49	1.80	1.07×10^{-6}	5.85×10^{-4}
NM_019012	PLEKHA5	Pleckstrin homology domain containing, family A member 5	Up	3.40	1.76	1.48×10^{-5}	8.66×10^{-6}
			Up	3.39	1.76	2.19×10^{-5}	1.29×10^{-5}
NM_005715	UST	Uronyl-2-sulfotransferase	Up	3.35	1.75	6.69×10^{-5}	4.10×10^{-5}
NM_152621	SGMS2	Sphingomyelin synthase 2	Up	3.35	1.75	5.20×10^{-5}	3.16×10^{-5}
NM_004994	MMP9	Matrix metallopeptidase 9	Up	3.33	1.74	9.61×10^{-5}	5.97×10^{-5}
NM_012223	MYO1B	Myosin IB	Up	3.33	1.74	2.24×10^{-5}	1.33×10^{-5}
NM_181342	FKBP7	FK506 binding protein 7	Up	3.29	1.72	1.05×10^{-4}	1.05×10^{-4}
NM_001542	IGSF3	Immunoglobulin superfamily, member 3	Up	3.26	1.71	1.45×10^{-4}	1.45×10^{-4}
NM_016848	SHC3	SHC (Src homology 2 domain containing) transforming protein 3	Up	3.24	1.70	3.12×10^{-5}	1.89×10^{-5}
	XLOC_005452		Up	3.23	1.69	2.96×10^{-5}	1.79×10^{-5}
NM_001124758	SPNS2	Spinster homolog 2 (Drosophila)	Up	3.22	1.69	4.51×10^{-5}	2.76×10^{-5}
NR_034143	CASC14	Cancer susceptibility candidate 14 (non-protein coding)	Up	3.22	1.69	4.80×10^{-6}	2.81×10^{-6}
	LINC00605	Long intergenic non-protein coding RNA 605	Up	3.15	1.66	4.86×10^{-5}	3.01×10^{-5}
NM_024312	GNPTAB	N-acetylglucosamine-1-phosphate transferase, alpha and beta subunits	Up	3.13	1.65	2.72×10^{-5}	1.66×10^{-5}
NM_018076	ARMC4	Armadillo repeat containing 4	Up	3.10	1.63	8.24×10^{-6}	4.96×10^{-6}
NM_005940	MMP11	Matrix metallopeptidase 11 (stromelysin 3)	Up	3.08	1.62	1.07×10^{-4}	1.07×10^{-4}
NM_014398	LAMP3	Lysosomal-associated membrane protein 3	Up	3.07	1.62	1.44×10^{-4}	1.44×10^{-4}
XM_006724937	LOC100132705	Immunoglobulin superfamily member 3-like	Up	3.06	1.61	8.57×10^{-5}	5.44×10^{-5}
NM_019854	PRMT8	Protein arginine methyltransferase 8	Up	3.00	1.58	6.46×10^{-5}	4.10×10^{-5}
TCONS_00030032			Up	2.96	1.57	2.28×10^{-5}	1.43×10^{-5}
NM_006307	SRPX	Sushi-repeat containing protein, X-linked	Up	2.94	1.55	1.15×10^{-5}	7.18×10^{-6}
NM_003034	ST8SIA1	ST8 alpha-N-acetyl-neuraminide alpha-2,8-sialyltransferase 1	Up	2.89	1.53	1.45×10^{-4}	9.54×10^{-5}
NM_017671	FERMT1	Fermitin family member 1	Up	2.89	1.53	7.22×10^{-5}	4.67×10^{-5}
NM_001081	CUBN	Cubilin (intrinsic factor-cobalamin receptor)	Up	2.88	1.53	1.24×10^{-5}	7.78×10^{-6}
NM_030794	TDRD3	Tudor domain containing 3	Up	2.85	1.51	6.78×10^{-6}	4.28×10^{-6}
XR_108587			Up	2.79	1.48	2.26×10^{-5}	1.46×10^{-5}
NM_000943	PPIC	Peptidylprolyl isomerase C (cyclophilin C)	Up	2.79	1.48	5.40×10^{-6}	3.47×10^{-6}
NM_005264	GFRA1	GDNF family receptor alpha 1	Up	2.75	1.46	8.36×10^{-5}	5.53×10^{-5}
NM_016184	CLEC4A	C-type lectin domain family 4, member A	Up	2.73	1.45	3.33×10^{-5}	2.18×10^{-5}
NM_001024630	RUNX2	Runt-related transcription factor 2	Up	2.72	1.44	1.55×10^{-5}	1.01×10^{-5}
NM_030801	MAGED4B	Melanoma antigen family D, 4B	Up	2.70	1.43	3.50×10^{-5}	2.31×10^{-5}
NM_001047	SRD5A1	Steroid-5-alpha-reductase, alpha polypeptide 1	Up	2.63	1.40	1.20×10^{-5}	8.05×10^{-6}
NM_003371	VAV2	Vav 2 guanine nucleotide exchange factor	Up	2.61	1.38	4.92×10^{-5}	3.32×10^{-5}
			Up	2.61	1.38	1.12×10^{-4}	7.63×10^{-5}

NM_033120	NKD2	Naked cuticle homolog 2 (Drosophila)	Up	2.58	1.37	1.23×10^{-4}	1.23×10^{-4}
NM_001037582	SCD5	Stearoyl-CoA desaturase 5	Up	2.58	1.37	1.39×10^{-4}	9.58×10^{-5}
NM_002773	PRSS8	Protease, serine, 8	Up	2.56	1.36	1.24×10^{-4}	8.54×10^{-5}
			Up	2.56	1.36	1.06×10^{-4}	1.06×10^{-4}
NM_001042481	FRMD6	FERM domain containing 6	Up	2.46	1.30	7.90×10^{-6}	5.66×10^{-6}
NM_181078	IL21R	Interleukin 21 receptor	Up	2.40	1.26	3.05×10^{-5}	2.19×10^{-5}
			Up	2.34	1.23	2.75×10^{-5}	2.02×10^{-5}
			Up	2.30	1.20	1.37×10^{-6}	1.15×10^{-6}
NR_104131	LINC01057	Long intergenic non-protein coding RNA 1057	Up	2.28	1.19	7.16×10^{-6}	5.64×10^{-6}
NM_004881	TP53I3	Tumor protein p53 inducible protein 3	Up	2.26	1.18	6.27×10^{-5}	4.71×10^{-5}
NM_001024736	CD276	CD276 molecule	Up	2.20	1.14	1.06×10^{-4}	8.11×10^{-5}
NM_183376	ARRDC4	Arrestin domain containing 4	Up	2.18	1.12	8.55×10^{-5}	6.60×10^{-5}
NM_006670	TPBG	Trophoblast glycoprotein	Up	2.17	1.12	6.44×10^{-6}	5.49×10^{-6}
NM_001031695	RBFOX2	RNA binding protein, fox-1 homolog (C. elegans) 2	Up	2.09	1.06	1.66×10^{-5}	1.43×10^{-5}
NR_034110	TRAF3IP2-AS1	TRAF3IP2 antisense RNA 1	Up	2.07	1.05	1.34×10^{-4}	1.34×10^{-4}
	ZNF815P	Zinc finger protein 815, pseudogene	Up	1.77	0.82	1.42×10^{-4}	1.44×10^{-4}
NM_000367	TPMT	Thiopurine S-methyltransferase	Up	1.75	0.81	1.09×10^{-4}	1.15×10^{-4}
AK091525			Up	1.74	0.80	4.75×10^{-5}	5.53×10^{-5}
NM_005765	ATP6AP2	ATPase, H+ transporting, lysosomal accessory protein 2	Up	1.64	0.71	4.90×10^{-5}	6.91×10^{-5}
NM_001605	AARS	Alanyl-tRNA synthetase	Down	-1.59	-0.67	5.46×10^{-5}	8.47×10^{-5}
NM_198679	RAPGEF1	Rap guanine nucleotide exchange factor (GEF) 1	Down	1.60	-0.68	1.19×10^{-4}	1.19×10^{-4}
NM_018093	WDR74	WD repeat domain 74	Down	-1.63	-0.71	3.77×10^{-5}	5.57×10^{-5}
NM_001039619	PRMT5	Protein arginine methyltransferase 5	Down	-1.64	-0.72	3.30×10^{-5}	4.86×10^{-5}
NM_016457	PRKD2	Protein kinase D2	Down	-1.66	-0.73	3.11×10^{-5}	4.46×10^{-5}
NM_006990	WASF2	WAS protein family, member 2	Down	-1.71	-0.77	1.06×10^{-4}	1.19×10^{-4}
XR_425288	LOC102725378	Uncharacterized LOC102725378	Down	-1.72	-0.78	1.33×10^{-4}	1.44×10^{-4}
NM_030927	TSPAN14	Tetraspanin 14	Down	-1.73	-0.79	1.27×10^{-4}	1.35×10^{-4}
NM_003768	PEA15	Phosphoprotein enriched in astrocytes 15	Down	-1.83	-0.87	1.45×10^{-4}	1.45×10^{-4}
NM_006058	TNIP1	TNFAIP3 interacting protein 1	Down	-1.83	-0.87	1.45×10^{-5}	1.66×10^{-5}
NM_002405	MFNG	MFNG O-fucosylpeptide 3-beta-N-acetylglucosaminyltransferase	Down	-1.83	-0.88	4.68×10^{-5}	4.79×10^{-5}
NM_052862	RCSD1	RCSD domain containing 1	Down	-1.85	-0.89	1.02×10^{-4}	9.60×10^{-5}
NM_001114618	MGAT1	Mannosyl (alpha-1,3-)-glycoprotein beta-1	Down	-1.87	-0.90	1.16×10^{-4}	1.08×10^{-4}
NM_015680	CNPPD1	Cyclin Pas1/PHO80 domain containing 1	Down	-1.89	-0.92	2.63×10^{-5}	2.64×10^{-5}
NM_006247	PPP5C	Protein phosphatase 5, catalytic subunit	Down	-1.90	-0.92	1.35×10^{-4}	1.35×10^{-4}
NM_000442	PECAM1	Platelet/endothelial cell adhesion molecule 1	Down	-1.92	-0.94	1.42×10^{-4}	1.25×10^{-4}
NM_014945	ABLIM3	Actin binding LIM protein family, member 3	Down	-1.96	-0.97	1.96×10^{-5}	1.87×10^{-5}
NM_001540	HSPB1	Heat shock 27kDa protein 1	Down	-2.00	-1.00	6.86×10^{-5}	5.90×10^{-5}
BC036832			Down	-2.00	-1.00	9.72×10^{-5}	8.23×10^{-5}
NM_003768	PEA15	Phosphoprotein enriched in astrocytes 15	Down	-2.03	-1.02	5.46×10^{-5}	4.66×10^{-5}
NM_138352	SAMD1	Sterile alpha motif domain containing 1	Down	-2.09	-1.07	1.19×10^{-4}	9.47×10^{-5}

NM_014220	TM4SF1	Transmembrane 4 L six family member 1	Down	-2.14	-1.10	3.01×10^{-5}	2.44×10^{-5}
NM_001166208	SYNPO	Synaptopodin	Down	-2.23	-1.16	6.94×10^{-5}	5.27×10^{-5}
NM_001243756	PXN	Paxillin	Down	-2.29	-1.19	2.39×10^{-5}	1.81×10^{-5}
NM_004415	DSP	Desmoplakin	Down	-2.29	-1.19	1.51×10^{-5}	1.16×10^{-5}
NM_002020	FLT4	Fms-related tyrosine kinase 4	Down	-2.30	-1.20	9.34×10^{-5}	6.87×10^{-5}
NM_152406	AFAP1L1	Actin filament associated protein 1-like 1	Down	-2.30	-1.20	5.35×10^{-6}	4.21×10^{-6}
NM_207627	ABCG1	ATP-binding cassette, sub-family G (WHITE), member 1	Down	-2.32	-1.21	3.92×10^{-6}	3.10×10^{-6}
NM_022153	C10orf54	Chromosome 10 open reading frame 54	Down	-2.34	-1.22	1.18×10^{-5}	8.85×10^{-6}
NM_080759	DACH1	Dachshund family transcription factor 1	Down	-2.34	-1.23	7.57×10^{-5}	5.51×10^{-5}
NM_007121	NR1H2	Nuclear receptor subfamily 1, group H, member 2	Down	-2.36	-1.24	7.64×10^{-5}	5.53×10^{-5}
NM_030927	TSPAN14	Tetraspanin 14	Down	-2.37	-1.25	6.56×10^{-5}	4.72×10^{-5}
NM_024726	IQCA1	IQ motif containing with AAA domain 1	Down	-2.41	-1.27	8.43×10^{-5}	6.01×10^{-5}
NM_001282714	FAM107A	Family with sequence similarity 107, member A	Down	-2.42	-1.27	1.19×10^{-4}	1.19×10^{-4}
NM_003064	SLPI	Secretory leukocyte peptidase inhibitor	Down	-2.49	-1.31	1.54×10^{-5}	1.08×10^{-5}
	XLOC_010730		Down	-2.50	-1.32	1.79×10^{-5}	1.25×10^{-5}
NM_201566	SLC16A13	Solute carrier family 16, member 13	Down	-2.58	-1.37	1.47×10^{-4}	1.47×10^{-4}
			Down	-2.61	-1.38	1.32×10^{-4}	9.03×10^{-5}
AF289611	LOC100128343	Uncharacterized LOC100128343	Down	-2.80	-1.49	1.43×10^{-4}	9.47×10^{-5}
NM_024726	IQCA1	IQ motif containing with AAA domain 1	Down	-2.92	-1.54	1.27×10^{-4}	8.29×10^{-5}
NM_024735	FBXO31	F-box protein 31	Down	-2.93	-1.55	5.56×10^{-5}	3.55×10^{-5}
NM_006613	GRAP	GRB2-related adaptor protein	Down	-3.11	-1.64	2.32×10^{-5}	1.42×10^{-5}
NR_110914	TP53TG3C	TP53 target 3C	Down	-3.38	-1.76	2.96×10^{-6}	1.67×10^{-6}
NM_006691	LYVE1	Lymphatic vessel endothelial hyaluronan receptor 1	Down	-3.61	-1.85	1.01×10^{-4}	6.16×10^{-5}
NR_027151	PRR26	Proline rich 26	Down	-3.71	-1.89	9.64×10^{-5}	9.64×10^{-5}
NM_004519	KCNQ3	Potassium voltage-gated channel, KQT-like subfamily, member 3	Down	-3.80	-1.93	2.24×10^{-5}	1.28×10^{-5}
	XLOC_001496		Down	-3.99	-2.00	1.45×10^{-4}	1.45×10^{-4}
NM_001066	TNFRSF1B	Tumor necrosis factor receptor superfamily, member 1B	Down	-4.03	-2.01	3.06×10^{-5}	1.74×10^{-5}
NM_002193	INHBB	Inhibin, beta B	Down	-4.12	-2.04	1.08×10^{-4}	1.08×10^{-4}
	ALU1	Alu 1 Element	Down	-5.02	-2.33	3.17×10^{-7}	1.44×10^{-7}
NM_025260	C6orf25	Chromosome 6 open reading frame 25	Down	-5.82	-2.54	5.35×10^{-6}	2.62×10^{-6}
NM_080429	AQP10	Aquaporin 10	Down	-6.92	-2.79	6.26×10^{-7}	2.62×10^{-6}
NM_005306	FFAR2	Free fatty acid receptor 2	Down	-7.29	-2.87	5.63×10^{-5}	3.06×10^{-5}
AB305916	TRBV28	T Cell Receptor Beta Variable 28	Down	-7.50	-2.91	3.35×10^{-6}	1.55×10^{-6}
NM_000517	HBA2	Hemoglobin, alpha 2	Down	-7.64	-2.93	7.61×10^{-7}	3.25×10^{-7}
	XLOC_014512		Down	-7.99	-3.00	2.74×10^{-7}	1.1×10^{-7}
NM_000517	HBA2	Hemoglobin, alpha 2	Down	-8.20	-3.04	5.59×10^{-7}	2.33×10^{-7}
NM_016509	CLEC1B	C-type lectin domain family 1, member B	Down	-8.24	-3.04	1.03×10^{-4}	2.33×10^{-7}
NM_002620	PF4V1	Platelet factor 4 variant 1	Down	-9.31	-3.22	2.34×10^{-6}	1.04×10^{-6}
NM_022468	MMP25	Matrix Metallopeptidase 25	Down	-9.33	-3.22	4.32×10^{-5}	2.28×10^{-5}
NR_120522	LOC102724484	Uncharacterized LOC102724484	Down	-10.04	-3.33	1.01×10^{-4}	5.6×10^{-5}

NM_001136503	SMIM24	Small integral membrane protein 24	Down	-10.29	-3.36	1.38×10^{-5}	6.73×10^{-6}
NM_030773	TUBB1	Tubulin, beta 1 class VI	Down	-12.37	-3.63	5.86×10^{-7}	2.34×10^{-7}
	HSJ1167H4		Down	-13.17	-3.72	3.71×10^{-6}	1.65×10^{-6}
NR_001552	TTTY16	Testis-specific transcript, Y-linked 16 (non-protein coding)	Down	-13.65	-3.77	6.28×10^{-5}	3.34×10^{-5}
NR_047499	LINC00570	Long intergenic non-protein coding RNA 570	Down	-14.00	-3.81	1.03×10^{-4}	8.67×10^{-5}
NM_144673	CMTM2	CKLF-like MARVEL transmembrane domain containing 2	Down	-14.25	-3.83	2.71×10^{-5}	1.36×10^{-5}
NM_001557	CXCR2	Chemokine (C-X-C motif) receptor 2	Down	-14.93	-3.90	9.27×10^{-6}	4.34×10^{-6}
NM_000519	HBD	Hemoglobin, delta	Down	-15.75	-3.98	7.89×10^{-8}	2.74×10^{-8}
NM_002100	GYPB	Glycophorin B (MNS blood group)	Down	-16.15	-4.01	1.03×10^{-4}	1.43×10^{-4}
XM_005261527	SEC14L3	SEC14-like 3 (S. cerevisiae)	Down	-16.65	-4.06	2.98×10^{-5}	1.5×10^{-5}
AK128128	FLJ46249		Down	-16.90	-4.08	6.19×10^{-5}	3.27×10^{-5}
NM_016509	CLEC1B	C-type lectin domain family 1, member B	Down	-17.06	-4.09	1.34×10^{-5}	6.39×10^{-6}
NM_016509	CLEC1B	C-type lectin domain family 1, member B	Down	-17.67	-4.14	4.83×10^{-6}	2.15×10^{-6}
NM_002049	GATA1	GATA binding protein 1 (globin transcription factor 1)	Down	-19.55	-4.29	7.87×10^{-5}	4.21×10^{-5}
NM_005764	PDZK1IP1	PDZK1 interacting protein 1	Down	-20.36	-4.35	7.59×10^{-6}	3.47×10^{-6}
NM_006163	NFE2	Nuclear factor, erythroid 2	Down	-22.54	-4.49	3.22×10^{-5}	1.62×10^{-5}
	XLOC_013489		Down	-23.69	-4.57	2.85×10^{-5}	1.42×10^{-5}
NM_002619	PF4	Platelet factor 4	Down	-31.42	-4.97	1.26×10^{-7}	4.32×10^{-8}
	XLOC_000346		Down	-31.94	-5.00	1.26×10^{-7}	2.56×10^{-5}
NM_000032	ALAS2	Aminolevulinate, delta-, synthase 2	Down	-33.49	-5.07	1.93×10^{-5}	9.3×10^{-6}
NM_005980	S100P	S100 calcium binding protein P	Down	-33.56	-5.07	1.11×10^{-4}	6.06×10^{-5}
NM_005331	HBQ1	Hemoglobin, theta 1	Down	-34.07	-5.09	3.58×10^{-6}	1.53×10^{-6}
NM_002704	PPBP	Pro-platelet basic protein (chemokine (C-X-C motif) ligand 7)	Down	-39.94	-5.32	4.11×10^{-8}	1.3×10^{-8}
NM_000517	HBA2	Hemoglobin, alpha 2	Down	-41.07	-5.36	2.47×10^{-7}	8.77×10^{-8}
NM_001003938	HBM	Hemoglobin, mu	Down	-45.11	-5.50	7.66×10^{-5}	4.05×10^{-5}
NM_018437	HEMGN	Hemogen	Down	-53.12	-5.73	1.89×10^{-6}	7.66×10^{-7}
NM_005621	S100A12	S100 calcium binding protein A12	Down	-56.95	-5.83	7.25×10^{-5}	3.81×10^{-5}
NM_005621	S100A12	S100 calcium binding protein A12	Down	-58.82	-5.88	4.6×10^{-5}	2.34×10^{-5}
NM_000559	HBG1	Hemoglobin, gamma A	Down	-88.82	-6.47	1.94×10^{-6}	7.82×10^{-7}

Accession #: Accession Number. Symbol: Entity Symbol. ↑↓: Regulation. Abs FC: Absolute Fold Change. Log FC: Log transformed Fold Change. P Value[a]: Adjusted Student T-test P value for microarray corrected for multiple testing by the Bonferroni FWER method. P Value[b]: Adjusted Moderated T-test P value for microarray corrected for multiple testing by the Bonferroni FWER method.